Exploring the role of cytochrome P450 family 1 subfamily B member 1 and quercetin in modulating neuropathic pain after spinal cord injury

PENGYU ZHOU[1], LU LI[1], YU CAO[1], JIAHAO CHEN[2], CHUYIN CHEN[2], XIANGSHENG ZHANG[1], JIURONG CHEN[1], YINGDONG DENG[1], ZIQIANG LIN[1], YUPEI LAI[1], SUO WANG[1], SIMIN TANG[1], WENQI ZHANG[3], PENG SUN[4,5] and JUN ZHOU[1]

[1]Department of Anesthesiology, The Third Affiliated Hospital of Southern Medical University, Guangzhou, Guangdong 510630, P.R. China; [2]Department of Anesthesiology, Shunde Hospital of Guangzhou University of Chinese Medicine, Foshan, Guangdong 528300, P.R. China; [3]Department of Anesthesiology, Hainan General Hospital (Affiliated Hospital of Hainan Medical University), Haikou, Hainan 570311, P.R. China; [4]Department of Anesthesiology, Sun Yat-Sen University Cancer Center, Guangzhou, Guangdong 510060, P.R. China; [5]State Key Laboratory of Oncology in South China, Collaborative Innovation Center for Cancer Medicine, Guangzhou, Guangdong 510060, P.R. China

Received March 14, 2025; Accepted August 28, 2025

DOI: 10.3892/mmr.2025.13717

Abstract. Spinal cord injury (SCI) represents a notable global health challenge, with neuropathic pain (NP) being a common complication that intensifies patient suffering. Existing research tends to overlook the temporal aspects of NP and fails to offer targeted treatment options. To tackle this issue, the present study initially examined genome-wide association study summaries related to NP, incorporating expression quantitative trait locus (eQTL) from blood samples through summary-based Mendelian randomization. This allowed the investigation of the association between NP and eQTL, facilitating the identification of genes linked to the risk of NP. Following this, weighted gene co-expression network analysis of a Gene Expression Omnibus dataset was utilized to identify SCI-related module genes, resulting in the detection of 218 shared genes across these analyses. Subsequent functional enrichment assessments, protein-protein interaction evaluations and machine learning technique analyses, including least absolute shrinkage and selection operator regression, random forest and support vector machine recursive feature elimination analyses, highlighted three central genes: Glycerol-3-phosphate dehydrogenase 1-like, epoxide hydrolase 2 and cytochrome P450 family 1 subfamily B member 1 (CYP1B1). Additionally, network pharmacology and molecular docking analyses confirmed CYP1B1 as a viable therapeutic target. A analysis of single-cell RNA sequencing datasets demonstrated an increase in CYP1B1 expression within spinal cord fibroblasts following SCI. Furthermore, quercetin (Que) was shown to inhibit CYP1B1 expression and reduce NP (based on mechanical paw withdrawal threshold and thermal paw withdrawal latency) in murine models. The results of the present study highlight the important role of spinal cord fibroblast CYP1B1 as a notable contributor to NP following SCI and suggest that Que may serve as a promising mechanism-based therapeutic option.

Correspondence to: Professor Jun Zhou, Department of Anesthesiology, The Third Affiliated Hospital of Southern Medical University, 183 Zhongshan Avenue West, Tianhe, Guangzhou, Guangdong 510630, P.R. China
E-mail: zhoujun7843@smu.edu.cn

Professor Peng Sun, Department of Anesthesiology, Sun Yat-Sen University Cancer Center, 651 Dongfeng Avenue East, Yuexiu, Guangzhou, Guangdong 510060, P.R. China
E-mail: sunpeng@sysucc.org.cn

Key words: spinal cord injury, neuropathic pain, Mendelian randomization, molecular docking and molecular simulation, cytochrome P450 family 1 subfamily B member 1, quercetin

Introduction

Spinal cord injury (SCI) is a prevalent etiology of central neuropathic pain (NP), with an estimated 40-70% of individuals with SCI experiencing this condition (1,2). NP represents a frequent and multifaceted secondary complication associated with SCI (3). The pathophysiological mechanisms underlying SCI-induced NP are complex, encompassing neuroplastic changes within the central nervous system, activation of immune cells, and the release of inflammatory mediators and cytokines (4-6). The manifestation of NP subsequent to SCI markedly influences patient outcomes, imposing notable psychological and economic burdens (2). Contemporary clinical approaches for the management of NP resulting from SCI predominantly encompass pharmacological interventions, including antiepileptic drugs, antidepressants and opioids, alongside neuromodulation techniques such as spinal cord stimulation, transcranial magnetic stimulation (TMS) and transcranial direct-current stimulation (tDCS) (7-9). Nonetheless, the mechanisms underlying the initiation and progression of NP post-SCI remain inadequately elucidated, and therapeutic strategies to mitigate SCI-induced NP remain insufficient.

Previous studies have shown that small molecules from traditional Chinese medicine could positively impact various diseases, with quercetin (Que) specifically exhibiting pain-relieving effects in NP (10,11). Animal models have demonstrated that Que can ease pain in a dose-dependent manner (12-14). Being a member of the flavonoid family, Que is found in fruits and vegetables such as apples, grapes and onions, and possesses antioxidant, anti-inflammatory, anti-aging and neuroprotective qualities (15-18). Research has demonstrated that Que can reduce oxidative stress and protect cells from inflammation-related damage, thus enhancing its neuroprotective properties (19,20). Although research on the impact of Que on NP following SCI is limited, exploring its therapeutic potential and understanding the mechanisms involved in the interactions of Que with NP is important.

Consequently, an integrative analysis was performed in the present study utilizing the largest available genome-wide association study (GWAS) summary data on NP, employing the summary-based Mendelian randomization (SMR) method. By conducting a further examination of publicly accessible RNA sequencing datasets, gene modules associated with SCI were identified. This methodology enabled genes common to both SCI and NP to be identified. Subsequently, by employing machine learning (ML) algorithms, molecular biomarkers that were indicative of NP subsequent to SCI were identified. In the present study, network pharmacology was utilized to predict the potential targets of Que, followed by molecular docking to assess the interaction between Que and these target proteins. The resulting protein-ligand complexes were further examined through molecular dynamics (MD) simulations to identify viable therapeutic targets for SCI-induced NP. This methodological approach offered novel insights and directions for future research on the biological mechanisms of SCI-induced NP and the development of targeted therapeutic strategies.

Materials and methods

Data acquisition and preprocessing. Fig. 1 illustrates the design of the present study. The present study was centered on trigeminal neuralgia (TN) and postherpetic neuralgia (PHN), two conditions that exemplify NP (1). The relevant datasets for these diseases were sourced from IEU OPENGWAS and FINNGEN (21,22). The GWAS identifiers for these datasets were finn-b-G6_POSTZOST and finn-b-G6_TRINEU, both of which are accessible for public download. Pooled statistics of blood expression quantitative trait locus (eQTL) were derived from the EQTLGEN dataset, which predominantly comprised blood samples from healthy European individuals. The EQTLGEN dataset included expression data for 16,987 genes, with gene expression quantified at the transcriptional level in peripheral blood (23).

A total of four publicly accessible transcriptome datasets were procured from the Gene Expression Omnibus database (https://www.ncbi.nlm.nih.gov/geo/). These datasets included: i) A human SCI dataset (GSE151371), which comprises blood samples from patients with SCI and healthy controls (24); ii) a single-cell SCI (ScSCI) dataset for mouse models (GSE162610) (25); iii) a mouse SCI model RNA dataset (GSE171441) (26); and iv) an RNA dataset from a mouse NP model using the spared nerve injury (SNI) model (GSE236754) (27). The downloaded raw RNA data were subjected to data quality control, processing and normalization in R (version 4.2.1; R Foundation for Statistical Computing; https://www.R-project.org/).

Screening of candidate genes

SMR and heterogeneity in dependent instruments (HEIDI) tests detect polytropic associations. The SMR test was employed to examine the association between exposure and outcome using instrumental variables (IVs), typically SNPs, as previously described (28). In summary, the study utilized cis-acting eQTL (cis-eQTL) genetic variation as an IV, with gene expression serving as the exposure factor, and PHN and TN as the outcomes. The Mendelian randomization (MR) approach was employed to estimate the effect of gene expression on NP. This estimation was derived by calculating the ratio of the estimated effect of cis-eQTL genetic variation on NP to its estimated effect on gene expression. This methodology was applied to integrate GWAS and eQTL pooled statistics, thereby facilitating the examination of pleiotropic associations between gene expression and NP. In the present SMR analysis, the main SNP selection criteria were based on the data processing procedures outlined on the official SMR website (https://yanglab.westlake.edu.cn/software/smr/#Overview). After downloading the data, the first step was to exclude SNPs with missing values according to these procedures, and the filtered data were then subjected to SMR analysis. The default settings in SMR were utilized, which included selecting SNPs within a 2 Mb distance from each individual probe as cis-eQTL, applying a PeQTL threshold of $<5x10^{-8}$ and excluding SNPs exhibiting very strong linkage disequilibrium ($r^2>0.9$) with the top-associated eQTL. The heterogeneity in dependent instruments (HEIDI) test was conducted to assess the presence of cascading relationships within the associations (28). A P_{HEIDI}-value >0.05 indicated that the original hypothesis was valid, suggesting the existence of a single causal variant among the observed associations. The F-statistic in the SMR analysis was computed using the formula $(b_eQ_{t1}/se_eQ_{t1})^2$. IVs exhibiting an F-statistic >10 were chosen for further evaluation. The SMR results, encompassing trajectory plots and effect plots, are accessible through the SMR webpage (https://yanglab.westlake.edu.cn/software/smr/#Overview). Genes related to TN and PHN were screened by SMR, and genes related to NP were identified by intersection.

Weighted gene co-expression network analysis (WGCNA) and modular gene selection. WGCNA is a systems biology approach employed to identify modules of highly correlated genes and to compute module membership measures. Utilizing the R package 'WGCNA' (version 1.73), co-expression networks were constructed and filtered based on an R^2 value >0.85. The appropriate 'soft' thresholding power (β), ranging from 1 to 20, was selected to ensure that the constructed co-expression networks conformed more closely to the characteristics of scale-free networks. Finally, utilizing Pearson's correlation coefficient and the P-value for each module trait, the network of SCI co-expression modules was derived and visualized to identify the shared genes within its key modules (29). Additionally, an online Venn diagram tool was employed to determine the intersecting genes between SCI and NP (30).

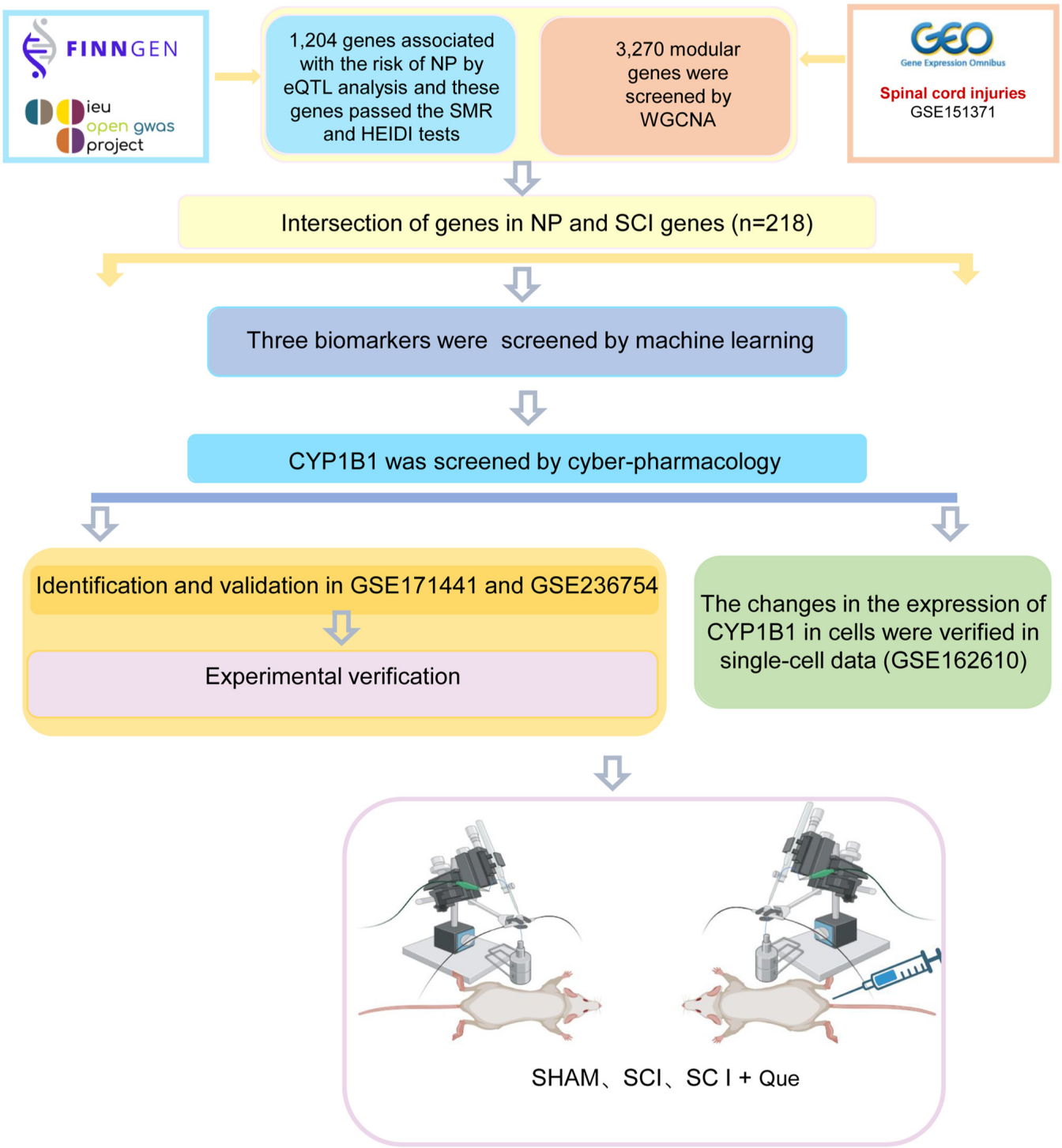

Figure 1. Research workflow. CYP1B1, cytochrome P450 family 1 subfamily B member 1; eQTL, expression-quantitative trait loci; HEIDI, heterogeneity in dependent instruments; NP, neuropathic pain; PPI, protein-protein interaction; Que, quercetin; SCI, spinal cord injury; SMR, summary-based Mendelian randomization; WGCNA, weighted gene co-expression network analysis.

Functional enrichment analysis. Both the Gene Ontology (GO) and Kyoto Encyclopedia of Genes and Genomes (KEGG) databases are accessible for the investigation of gene functions (31,32). To further investigate the role of genes implicated in NP following SCI, an online Venn diagram tool was utilized to identify intersecting genes between NP-related candidate genes and key module genes associated with SCI. Subsequently, GO and KEGG functional enrichment analyses were conducted using the 'clusterProfiler' package (version 4.14.6), with a significance threshold set at $P<0.05$. Both the visualization of enrichment analysis results and the generation of the Upset plot were performed using the Hiplot (ORG) (https://hiplot.org) (33).

Protein-protein interaction (PPI) network construction and identification of hub genes. Based on the identified intersecting genes, a minimum interaction score of 0.400 was established using the STRING database

(version 12.0) to investigate protein-coding gene interactions (34). Subsequently, the visualization of PPI networks was performed using Cytoscape (version 3.9.1) (35). To evaluate and identify hub genes, seven commonly used algorithms, 'maximal clique centrality', 'measurement coefficient network', 'degree', 'embedding pathway components', 'closeness', 'radiality' and 'stress', were employed using the cytoHubba plug-in in Cytoscape.

Immune infiltration analysis. The immune infiltration analysis utilized single sample gene set enrichment analysis to assess the relative abundance of specific immune cell types in each sample. Enrichment scores for a reference set of 28 unique immune cell types were calculated to reveal infiltration patterns across the samples (36,37). The associations between genes and immune cells were subsequently visualized utilizing the 'ggplot2' (version 3.5.1; https://ggplot2.tidyverse.org/) and 'ggExtra' (version 0.10.1; https://cran.r-project.org/package=ggExtra) R packages, facilitating a comprehensive depiction of gene-immune cell relationships.

Identification of disease marker genes through ML. Gene screening for disease diagnosis can be enhanced through the combined application of ML algorithms, including least absolute shrinkage and selection operator (LASSO), support vector machine recursive feature elimination (SVM-RFE) and random forest (RF) algorithms, for feature selection. LASSO is a regression technique that selects variables to enhance both the predictive accuracy and interpretability of statistical models (38). In the current investigation, a 10-fold cross-validation approach was employed, guided by the 'lambda.min' criterion, to derive the final gene set utilizing the 'lambda.min' value. SVM-RFE, an ML algorithm, was employed for gene selection by ordering features using a linear support vector machine (SVM) (39). The RF algorithm is classified under supervised learning models and functions as an ensemble tree-based ML tool that enhances prediction accuracy by averaging values from a subset of each tree (40). In the RF algorithm, the total 'ntree' value was configured to be 500. Additionally, the Boruta feature selection significance threshold was established at a P-value of 0.01, with a maximum of 300 iterations. Furthermore, the proportion of training datasets for the purpose of database segmentation was determined through the utilization of the 'createDataPartition' function. SVM-RFE, LASSO regression and RF analyses were conducted utilizing the R function packages 'glmnet' (version 4.1-8) (41), 'randomForest' (version 4.7-1.2) (42) and 'e1071' (version 1.7-16) (43). Genes identified through SVM, LASSO and RF analyses were deemed to be potential key markers for SCI diagnosis. To assess the association between candidate hub genes implicated in SCI diagnosis and NP, the Comparative Toxicogenomics Database (CTD) (https://ctdbase.org/) was utilized to extract genes associated with NP importance scores. Consequently, the hub genes most pertinent to NP in the context of SCI diagnosis were identified.

Identification of SCI subtypes was performed by non-negative matrix factorization (NMF) clustering of pain-related genes. The NMF algorithm is an innovative ML algorithm that identifies and clusters molecular function patterns from high-throughput data (44). The NMF approach was applied to samples using the 'NMF' R package (version 0.26) (45) to identify subtypes of SCI within various NP-related gene expression profiles derived from SMR.

Column chart construction and assessment of receiver operating characteristic (ROC) curve. The construction of column graphs is important in the clinical diagnosis of SCI. In the present study, the 'rms' R package (version 7.0-0; https://cran.r-project.org/package=rms) was utilized to generate a column chart based on candidate genes. The 'Points' denote the scores assigned to each candidate gene, while the 'Total Points' represent the aggregate score of all candidate genes. Subsequently, the 'pROC' R package (version 1.18.5; https://github.com/xrobin/pROC) was employed to construct a ROC curve (46), which was used to evaluate the diagnostic efficacy of the candidate genes in SCI diagnosis. The diagnostic value was quantified by calculating the area under the curve (AUC) along with its 95% CI. Typically, an AUC >0.7 is regarded as an acceptable diagnostic threshold.

Network pharmacology

Screening for potential targets of Que. The Simplified Molecular Input Line Entry System notation for Que constituents was obtained from the PubChem database (https://pubchem.ncbi.nlm.nih.gov/) and entered into the Swiss Target Prediction tool to identify potential targets with a probability of ≥0.4 (http://www.swisstargetprediction.ch/) (47).

Molecular docking. CYP1B1 was selected as the receptor for Que. The molecular structure and 'MOL2' format of Que were obtained from the Chinese Traditional Medicine Systems Pharmacology database (https://old.tcmsp-e.com/tcmsp.php), while the protein structure and Protein Data Bank (PDB) format of CYP1B1 were obtained from the PDB database (https://www.rcsb.org/). Finally, ligand-receptor-related file formats were imported into the AutoDock software (version 1.5.7) to perform docking, thereby generating docking fractions and facilitating the analysis of protein active sites (48,49). Subsequently, these results were imported into the PYMOL software (version 2.6.0a0; https://pymol.org/) for the visualization, display and detailed analysis of molecular structures (50).

MD simulation. MD simulations of the Que-CYP1B1 complex were conducted utilizing the Groningen machine for chemical simulations software version 2020.6 (https://www.gromacs.org/). The simulations employed the 'AMBER99SB' force field in conjunction with the simple point charge water model, maintaining the system at a temperature of 300 K over a duration of 40 nsec. Initially, energy minimization was achieved through the application of the conjugate gradient method, which was followed by a canonical ensemble equilibration step to ensure system stabilization. The MD simulation was then executed to completion. The resulting simulation data were analyzed and visualized using Qtgrace software (version 0.2.6; https://sourceforge.net/projects/qtgrace/).

Validation

Validation of external datasets pertaining to diagnostic hub genes and single-cell sequencing analysis. The mRNA expression of the identified NP-associated key SCI diagnosis genes was validated using the GSE171441 and GSE236754 datasets. The GSE171441 dataset comprised 3 control samples and 3 SCI samples, while the GSE236754 dataset included 12

control samples and 12 SNI samples. An unpaired t-test-test was used to compare control and trial group data, and $P<0.05$ was considered to indicate a statistically significant difference. Additionally, to identify potential targets of Que and assess the relevance of NP-related hub genes and cells in the context of SCI, the single-cell GSE162610 dataset was analyzed using the 'Seurat' R package (version 5.2.1; https://satijalab.org/seurat/) (51). Initially, the 'PercentageFeatureSet' function was employed to calculate the proportion of mitochondrial genes in each cell. The cells were then filtered by creating separate objects for each sample, retaining only those cells with <10% mitochondrial gene content and >50 gene expression counts. Subsequently, multiple samples were integrated using canonical correlation analysis (52,53). A total of 3,000 highly variable genes were selected for analysis, and appropriate principal component values and resolution parameters were chosen to obtain cell clusters, which were subsequently visualized using the 'uwot R package (version 0.2.3; https://cran.r-project.org/package=uwot). Subsequently, the analyzed clusters were annotated by integrating the results of the corresponding marker genes from the PanglaoDB database (54) and the CellMarker database (55). Finally, the 'ggplot2' R package (version 3.5.1; https://ggplot2.tidyverse.org/) was employed for the subsequent visualization of the single-cell sequencing analysis results.

Construction of the SCI model. The study was in compliance with the Guidelines for the Care and Use of Experimental Animals (https://portal.smu.edu.cn/sydwzx/fgbz/3.htm) and approved by the Ethics Committee of the Third Affiliated Hospital of Southern Medical University and the Animal Experimental Committee of the Daoke Pharmaceutical Technology (Guangdong) Co., Ltd. (approval no. IACUC-DK-2024-04-10-01). Male C57BL6J mice (6-8 weeks old; mean body weight, 25 g; Huaxia Cage Biotechnology Co., Ltd.), underwent standardized rearing in an SPF animal house (temperature, 22±2˚C; relative humidity, 55±5%; 12-h light-dark cycle) with daily monitoring of environmental parameters, replacement of litter and replenishment of food and water every 48-72 h. The mice were randomly allocated into three experimental groups, each consisting of 20 subjects (n=20 per group): The sham-operated (SHAM) control group, which underwent anesthesia, laminectomy and all surgical procedures except for the induction of SCI, the SCI group and the SCI combined with Que treatment group (SCI + Que). In the present study, C57BL/6J strain mice were anesthetized by intraperitoneal administration of a 1.25% solution of tribromoethanol (commercially known as Avertin (cat. no. 75-80-9; Sigma-Aldrich; Merck KGaA) at a dose of 250 mg/kg. In the present study, Avertin was used only prior to model construction and euthanasia. The mice were anesthetized using Avertin™ and subjected to a laminectomy at the T10 vertebral level to expose the T9-T10 segment of the spinal cord. SCI was induced via a controlled contusion at the T9 segment, utilizing a spinal impactor with the following parameters: i) Impact velocity of 1.5 m/sec; ii) impact depth of 0.2 mm; iii) dwell time of 0.5 sec; and iv) hammer diameter of 1.3 mm. Post-surgical procedures involved suturing the skin and muscle, followed by placing the mice on a heating pad to promote recovery. Manual bladder expression was conducted twice daily for a duration of 2 weeks to aid in urination. Furthermore, all mice were administered intraperitoneal injections of the antibiotic cefotaxime (cat. no. 64485-93-4; Sigma-Aldrich; Merck KGaA) at a dosage of 16 mg/kg, administered twice daily over a period of 7 days. Mice in the SCI + Que group received Que (cat. no. hy-18085; MedChemExpress) injections twice daily at a dose of 7.5 mg/kg for 14 days. This dose was specifically selected based on previous studies (56,57). Motor function was evaluated using the Basso Mouse Scale (BMS) on post-operative days 1, 3, 7, 10 and 14. The BMS scoring system categorizes motor function as follows: i) A score of 0 signifies total paralysis; ii) scores ranging between 1 and 3 reflect mild movement capabilities; iii) scores of 4-5 denote the presence of a plantigrade gait; iv) scores from 6 to 8 indicate coordinated walking abilities; and v) a score of 9 represents normal motor function (58). Additionally, on postoperative day 14, the mechanical paw withdrawal threshold (MWT) and thermal paw withdrawal latency (TWL) were assessed in the hind paws of mice from each experimental group. MWT was determined using a set of calibrated Von Frey aesthesiometers (KW-CT-1; KEW BASIS; Nanjing Calvin Biotechnology Co., Ltd.), and the TWL was measured using the Plantar Test (Hargreaves method) with heated glass (part no. 390G; IITC, Inc.). The mice were anesthetized with 250 mg/kg of Avertin and then euthanized by cervical dislocation. Death was confirmed by the absence of cardiac or respiratory activity for at least 5 min post-mortem, along with no response to painful stimuli.

Cell culture. Fibroblasts of the NRK-49F cell line (cat. no. CL-0854; Procell Life Science & Technology Co., Ltd.) were maintained in Dulbecco's modified Eagle's medium (DMEM; Invitrogen; Thermo Fisher Scientific, Inc.) supplemented with 10% fetal bovine serum (FBS; FSP500; Shanghai ExCell Biology, Inc.) and 1% penicillin-streptomycin under standard conditions at 37˚C with 5% CO_2. The fibroblasts were seeded at a density of $2x10^5$ cells/ml and allocated into three experimental groups (n=4 per group): i) Control (Con) group; ii) group treated with 10 ng/ml TGF-β; and iii) group treated with 10 ng/ml TGF-β in combination with 10 μmol/ml Que (TGF-β + Que). Each group was subjected to the respective treatments for a duration of 24 h.

Western blotting. NRK-49F cells and mouse spinal cord tissue samples were lysed using a lysis buffer containing a protease inhibitor cocktail (Beyotime Institute of Biotechnology). Protein concentration was determined using the BCA protein assay kit (cat. no. 23227; Thermo Fisher Scientific, Inc.). The protein samples were then transferred to polyvinylidene fluoride membranes, which were subsequently blocked for 1 h at room temperature., washed with TBST solution and incubated with the following primary antibodies: CYP1B1 (1:500; cat. no. 18505-1-AP; Proteintech Group, Inc.), Fibronectin (Fn) (1:1,000; cat. no. ab2413; Abcam) and GAPDH (1:50,000; cat. no. 1E6D9; Proteintech Group, Inc.). The membrane was incubated with primary antibodies overnight at 4˚C. The following day, after washing, it was incubated with horseradish peroxidase (HRP)-conjugated goat anti-rabbit IgG (1:5,000; cat. no. ab205718; Abcam) and goat anti-mouse IgG (1:5,000; cat. no. ab150113; Abcam) for 1 h at room temperature. Protein detection was performed using the Biodlight™ ECL Chemiluminescent HRP Substrate (High Sensitivity) (cat. no. BLH01S100; Bioworld Technology, Inc.) and a TANON-5200 Chemiluminescent Imaging System

(Tanon Science and Technology Co., Ltd.). Results analysis was performed using ImageJ software (version 1.54 g; National Institutes of Health) and Prism (version 9.0.0; Dotmatics).

Reverse transcription-quantitative PCR (RT-qPCR). Total RNA was isolated from spinal cord tissue and fibroblasts utilizing Trizol reagent (cat. no. bs258A; Biosharp Life Sciences). After verifying RNA purity, complementary DNA (cDNA) synthesis was performed using the HiScript II Q RT SuperMix for qPCR kit (cat. no. R222-01; Vazyme Biotech Co., Ltd.) according to the manufacturer's instructions. The reverse transcription procedure was carried out under the following conditions: 50˚C for 15 min, 85˚C for 5 sec, followed by a hold at 4˚C. qPCR was subsequently performed with the ChamQ Universal SYBR qPCR Master Mix kit (cat. no. Q711-02; Vazyme Biotech Co., Ltd.). The amplification protocol consisted of an initial phase for 1 min at 95˚C, followed by 50 cycles for 15 sec at 95˚C and 30 sec at 50˚C. The relative mRNA expression levels of the target genes were normalized to GAPDH expression levels and analyzed using the $2^{-\Delta\Delta Cq}$ method (59). Details of the primer sequences are shown in Table SI, and the rat primers included in the table are for cell experiments only.

Immunofluorescence. After euthanasia, the spinal cords were removed and washed in PBS. The spinal cords were immersed in a 4% glutaraldehyde solution at 4˚C for 24 h for fixation, followed by cryoprotection in a sucrose solution for 48 h at 4˚C. Using a cryostat, the spinal cords were manually sectioned into 10-μm-thick slices for immunofluorescence staining. The slides were allowed to equilibrate at room temperature for 1 h. Subsequently, 0.5% Triton X-100 permeabilization solution (cat. no. 9036-19-5; Sigma-Aldrich; Merck KGaA) was applied to the sections and incubated at 4˚C for 5 min. Ready-to-use goat serum blocking buffer (Beyotime Institute of Biotechnology) was then applied, followed by incubation at room temperature for 1 h. The sections were incubated overnight at 4˚C with the following primary antibodies: CYP1B1 (1:100 dilution; cat. no. 18505-1-AP; Proteintech Group, Inc.) and PDGF-D (1:100 dilution; cat. no. 14075-1-AP; Proteintech Group, Inc.). Afterward, the sections were stained for 1 h with the following secondary antibodies: Goat anti-mouse IgG H&L (1:500; cat. no. ab150113; Abcam) and goat anti-rabbit IgG H&L (1:500; cat. no. ab150080; Abcam). Finally, cell nuclei in the tissue sections were labeled using 4',6-diamidino-2-phenylindole (cat. no. F6057; Sigma-Aldrich; Merck KGaA). The stained samples were visualized under an upright fluorescence microscope (Olympus Corporation), and images were analyzed using ImageJ software. Three replicates were conducted for the immunofluorescence experiments to ensure the reliability and reproducibility of the results of the present study. Furthermore, spinal cord tissues were collected from six independent mice per group to account for inter-individual variability. Additionally, serial sections from the same tissue block were stained separately on different days to control for batch effects. Furthermore, ImageJ (National Institutes of Health) was used to quantify fluorescence intensity by measuring the mean pixel intensity of the regions of interest. To ensure accuracy, the fluorescence intensity data were normalized to sham group samples to account for variations in imaging conditions.

Statistical analysis. In the present study, R (version 4.2.1, R Foundation for Statistical Computing; https://www.R-project.org/) was used as the core analysis tool, and Prism 9.0 was used for all data statistics. The data presented are from three independent experiments. During hypothesis testing, each value is presented as mean ± SEM. For comparative analysis of different data structures, two groups were compared using an independent samples t-test. Multiple groups were compared using one-way ANOVA, followed by the Tukey's honest significant difference post hoc test. The Kruskal-Wallis test was applied for the BMS scores, followed by Dunn's post hoc test. The resulting figure was visualized using Adobe Illustrator (version 24.0; https://www.adobe.com/products/illustrator.html). $P<0.05$ was considered to indicate a statistically significant difference.

Results

NP-related genes identified using SMR, and the key module genes associated with SCI determined through WGCNA. Prioritization was achieved through WGCNA, utilizing the SMR and HEIDI methods to identify pleiotropic associations between gene expression and both TN and PHN. To mitigate the effects of pleiotropy and improve the precision of causal inference, cis-eQTLs were exclusively used as genetic instruments. The SMR results, following HEIDI testing, revealed associations with 610 genes for TN (Fig. 2A) and 619 genes for PHN (Fig. 2B). In the present study, the most pertinent modules related to SCI were analyzed using WGCNA. Based on this threshold, 13 distinct gene co-expression modules were identified, with each module represented by a different color (Fig. 2C). The analysis revealed that selecting a 'soft' thresholding power β of 20 (scale-free R^2, 0.85) resulted in gene associations that most closely adhered to a scale-free distribution (Fig. 2D and E). Pearson's correlation analysis revealed that the MEpink module (correlation coefficient r, 0.77), the MElightgreen module (correlation coefficient r, -0.75) and the MEgreen module (correlation coefficient r, 0.73) exhibited strong correlations with SCI (Fig. 2F). Consequently, modules with correlation coefficients >0.70 were identified as key modules for subsequent SCI analyses. This selection process resulted in a total of 3,243 genes identified across the three key modules (Fig. 2G-I).

Core gene screening and immune infiltration analysis. The aforementioned NP-related candidate genes were cross-referenced with key module genes associated with SCI, resulting in the identification of 218 intersecting genes (Fig. 3A). By applying seven different algorithms implemented by the cytoHubba plug-in in Cytoscape, the top 45 genes for each algorithm's respective score were identified. Following the intersection analysis using a Upset plot, 21 hub genes were identified (Fig. 3B). These 218 genes subsequently underwent GO and KEGG enrichment analyses (Fig. 3C). The GO enrichment analysis revealed that the intersecting genes were predominantly associated with biological processes such as 'response to toxic substance', 'response to oxidative stress' and 'regulation of neuron apoptotic process'. In the context of cellular component ontology, notable enrichment was observed in the 'mitochondrial matrix' and 'ion channel complex'. Molecular

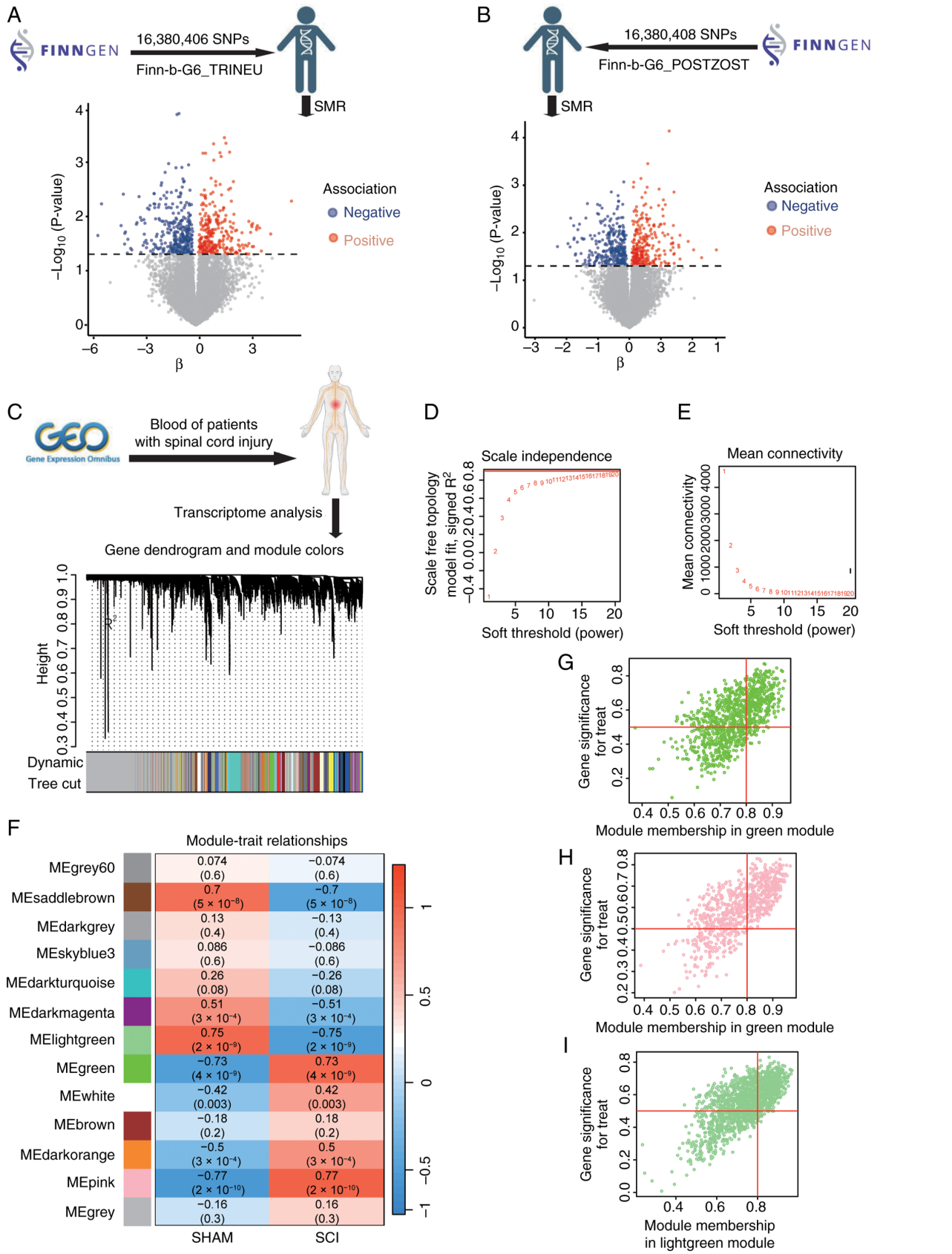

Figure 2. (A) Volcano plot showing 610 genes associated with trigeminal neuralgia. (B) Volcano plot showing 619 genes associated with post-herpetic neuralgia. Genes positively correlated with the disease are marked in red and genes negatively correlated with the disease are marked in blue. (C) Co-expression modules of genes represented by different colors under the gene tree. (D) The scale-free topology model fit (y-axis, signed R^2) against different soft threshold (power) values (x-axis). (E) The mean connectivity (average number of connections per gene, y-axis) vs. the soft threshold (power) (x-axis). (F) Heatmap of module-trait relationships in SCI, with each unit of a different module containing the corresponding correlation and P-value. (G) Green Module: Correlation between module membership and gene significance for treatment. (H) Pink module: Correlation between module membership and gene significance for treatment. (I) Light green module: Correlation between module membership and gene significance for treatment. SCI, spinal cord injury; SHAM, sham surgery group; SMR, summary-based Mendelian randomization; SNP, short nucleotide polymorphism.

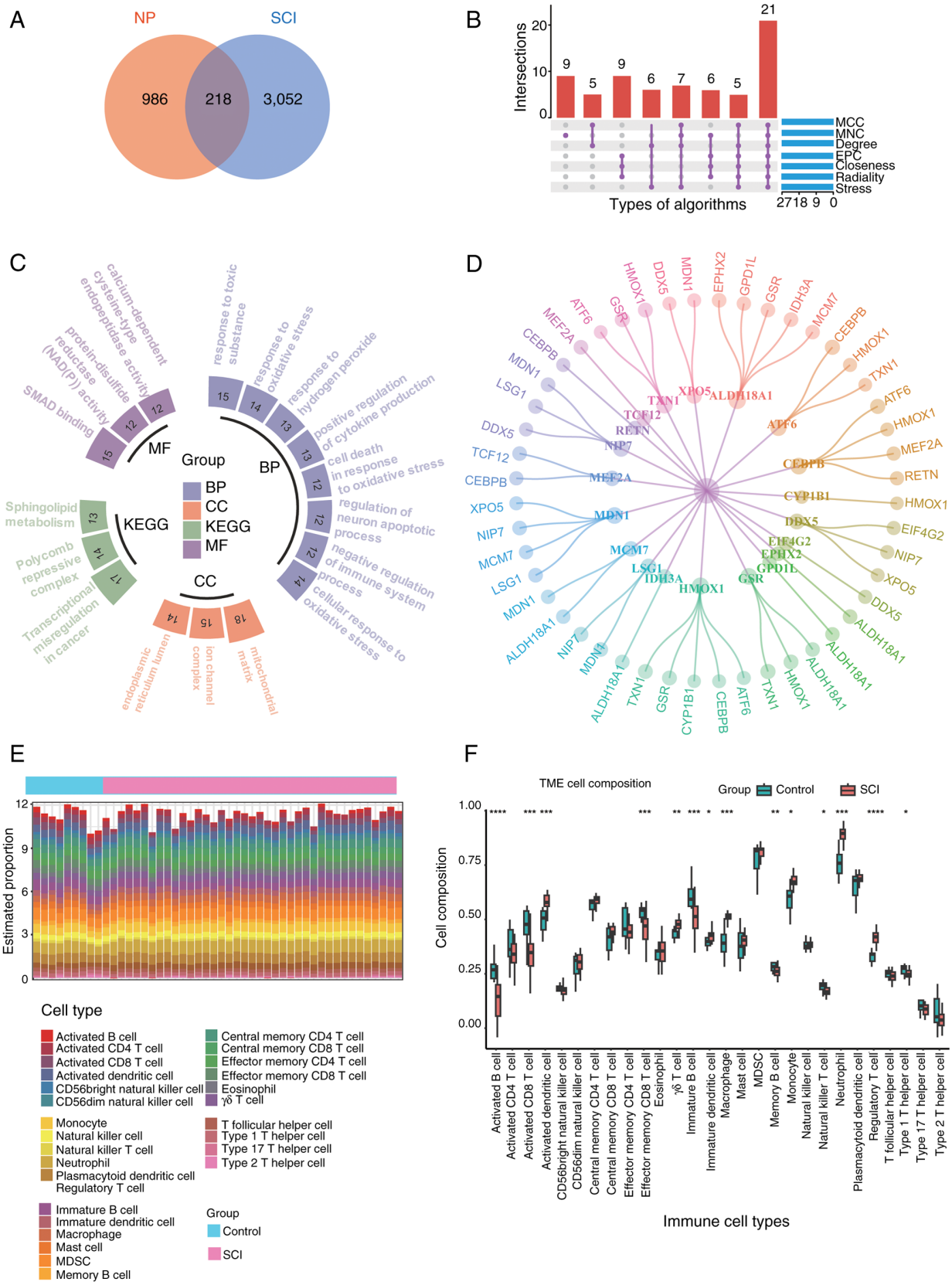

Figure 3. (A) Venn diagram obtained by crossing NP-related candidate genes with SCI key module genes, with a total of 218 common genes. (B) Upset plot depicting the intersection of the top 45 genes produced by each of the seven algorithms to get 21 genes. (C) Results of GO and KEGG enrichment analysis of 218 common genes. Different colors represent the classification of different enrichment pathways, including KEGG, and BP, CC and MF in GO, with P<0.05 for all enriched pathways, and the number of each bar cell represents the Count. (D) Protein-protein interaction network diagram of the 21 core genes (there are only 20 gene interactions in the image as the gene ALOX5AP cannot be identified by the SRING database). (E) Proportions of 28 immune cell types in different samples are shown in the bar graph. (F) Comparison of the proportions of 28 immune cell types in SCI and control groups. *P<0.05, **P<0.01, ***P<0.001 and ****P<0.0001 vs. control. BP, biological processes; CC, cellular component; GO, Gene Ontology; KEGG, Kyoto Encyclopedia of Genes and Genomes; MF, molecular function; NP, neuropathic pain; SCI, spinal cord injury; TME, tumor microenvironment; MCC, maximal clique centrality; MNC, measurement coefficient network; EPC, embedding pathway components.

function analyses indicated that the intersecting genes were predominantly enriched in 'protein-disulfide reductase (NAD(P)) activity', 'SMAD binding' and 'calcium-dependent cysteine-type endopeptidase activity'. Regarding the KEGG pathway analysis, notable enrichment was found in 'transcriptional misregulation in cancer', 'polycomb repressive complex' and 'sphingolipid metabolism'. The 218 intersecting genes were subsequently analyzed to determine potential interactions among their encoded proteins using the STRING database. In order to explore the protein-protein interaction of these 21 genes, PPI interaction experiments were carried out (Fig. 3D). The observations of the analysis indicated that genes associated with NP were implicated in the pathogenesis of SCI. Enrichment analysis revealed notable involvement in immune system regulation. Consequently, immune infiltration analysis may provide deeper insights into the immune regulatory mechanisms underlying SCI. The bar graph in Fig. 3E illustrates the proportion of 28 immune cell types in each sample for both patients with SCI and control subjects in the GSE151371 dataset. According to the vioplot analysis, patients with SCI exhibited elevated levels of activated dentritic cell, γδ T cells, immature dendritic cells, macrophages, monocytes, neutrophils and regulatory T cells compared with controls. Conversely, the levels of activated B cells, activated CD8 T cells, effector memory CD8 T cells, immature B cells, memory B cells, natural killer cells and type 1 T helper cells were found to be lower in patients with SCI than in controls (Fig. 3F).

Identification of the diagnostic marker gene CYP1B1. The pivotal genes were identified through the application of LASSO regression, SVM-RFE and RF ML algorithms, which facilitated the construction of column-line diagrams and the assessment of diagnostic value. LASSO regression identified 10 potential diagnostic candidate genes (Fig. 4A and B), while the SVM-RFE algorithm identified 11 potential diagnostic candidate genes (Fig. 4C). The RF algorithm ranked the 21 genes identified at the intersection of seven algorithms. From this ranking, the top 15 most diagnostic candidate genes were selected. (Fig. 4D). The potential diagnostic candidate genes identified through three ML algorithms were visualized using a Venn diagram (Fig. 4E), leading to the selection of three genes, CYP1B1, EPHX2 and GPD1L, for further investigation. Subsequently, a nomogram was developed (Fig. 4F) utilizing these three diagnostic candidate genes. ROC curves were constructed for the aforementioned genes to evaluate their diagnostic specificity and sensitivity. The AUC of CYP1B1 was 0.953 with a CI of 0.876-1.000 and an optimal cut-off of 3.615 (Fig. 4G), the AUC of EPHX2 was 0.989 with a CI of 0.961-1.000 and an optimal cut-off of 1.167 (Fig. 4H), and the AUC of GPD1L was 0.957 with a CI of 0.862-1.000 and an optimal cut-off of 2.292 (Fig. 4I). These findings suggest that CYP1B1, EPHX2 and GPD1L possess significant diagnostic value for SCI. The association between three identified candidate genes for SCI diagnosis and neuralgia disease was investigated by using the inference score of neuralgia disease with CTD (https://ctdbase.org/). Among them, CYP1B1 exhibited the highest inference score, suggesting a stronger association with pain (Fig. 4J). As a result, CYP1B1 was selected as a target gene in the blood for further investigation of its association with NP risk through MR analysis. Additionally, the gene CDC42 effector protein 3, located within a 2 Mb window of CYP1B1, was identified to be associated with NP risk (Fig. 5A and B).

Screening and identification of target genes for Que. Fig. 5C depicts the chemical structure of Que. Employing a network pharmacology methodology, 100 potential gene targets of Que were identified. This analysis revealed that CYP1B1 was implicated not only in the pathogenesis of NP following SCI but also as a potential therapeutic target for Que.

Molecular docking of Que and CYP1B1. Molecular docking experiments were conducted to further investigate the interaction between CYP1B1 and Que, revealing a binding energy of -8.9 kcal/mol for Que with CYP1B1 (Fig. 5D and E). The intersections of these potential targets with 21 core genes were analyzed using a Venn diagram (Fig. 5F). The binding affinity of both entities was determined to be <-5 kcal/mol, indicating a notable affinity of Que for CYP1B1. The interaction bond between Que and CYP1B1 is represented in Fig. S1A. Furthermore, negative control substances that exhibit anti-inflammatory properties and possess a comparable molecular weight to Que, specifically paracetamol, aspirin and caffeine, were incorporated. In the present investigation, The aforementioned negative control reagents were docked with CYP1B1. Although the binding energies of the control reagents with CYP1B1 were <-5 kcal/mol, Que exhibited the strongest binding affinity, as indicated by the most negative binding energy. This is one of the reasons why Que was chosen for follow-up. The detailed molecular docking results are shown in Fig. S1B.

MD simulation study of the Que-CYP1B1 complex. To further validate the binding affinity and stability of Que with CYP1B1, a 40 nsec MD simulation was conducted to assess the docking results. The root mean square deviation (RMSD) is a dependable measure for assessing the stability of protein-ligand conformations, as it indicates changes in atomic positions compared with the original structure. Greater stability is indicated by a lower RMSD value. As depicted in Fig. 5G and H, the Que-CYP1B1 complex achieved equilibrium after 15,000 psec, with RMSD fluctuations stabilizing at ~1.25 Å, and the radius of gyration (Rg) exhibited only slight variations during the simulation, suggesting that the interaction between Que and CYP1B1 is highly stable. The flexibility of the amino acid residues of the protein was assessed using the root mean square fluctuation (RMSF). As illustrated in Fig. 5I, the RMSF values were relatively low (predominantly <1 Å), indicating high stability. Additional analysis revealed that the solvent-accessible surface area fluctuated between 395 and 425 Å^2 during the simulation (Fig. 5J), suggesting that the structure of the protein remained relatively stable after ligand attachment. Using RMSD and Rg values, the Gibbs relative free energy was used to create a free energy landscape, with RMSD, Rg and Gibbs free energy plotted on the X, Y and Z axes. The free energy landscape outlines the lowest energy conformations seen during the MD simulation of the complex, as shown in Fig. 5K. The blue points represent the lowest energy values, which correspond to the most stable structural shapes. The Que-CYP1B1 complex demonstrated a nearly

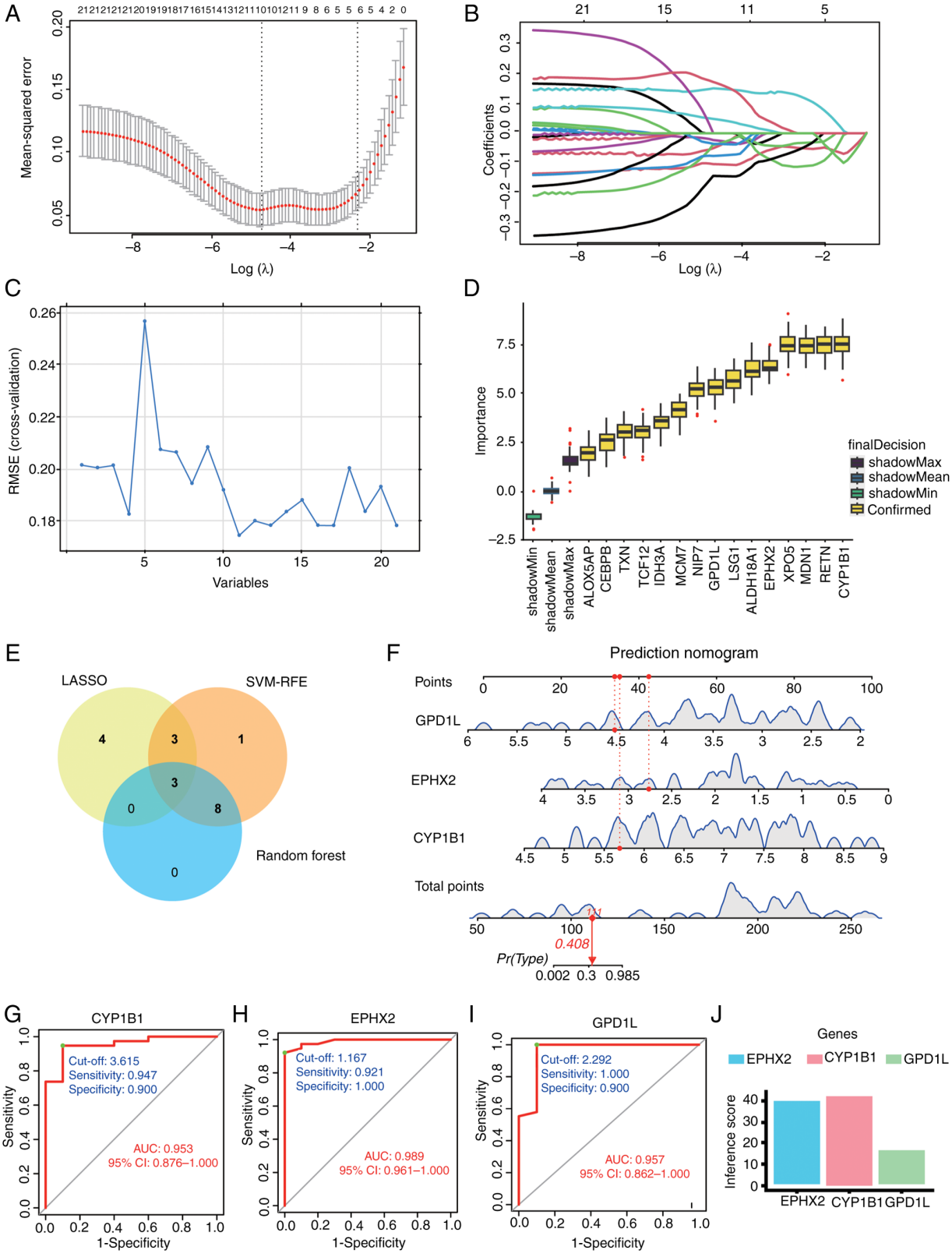

Figure 4. (A) Screening of diagnostic marker genes in the LASSO model. This panel shows the cross-validated mean-squared error plotted against Log(λ). The number of genes corresponding to the lowest point of the curve (n=10) was most suitable for the diagnosis of SCI. (B) This panel displays the number of features (variables) retained in the model at different values of Log(λ). (C) Characteristic gene selection using the SVM-RFE technique. A total of 11 characteristic genes were identified from the 21 core genes. (D) The 15 trait genes were ranked according to the importance score. (E) Venn diagram of diagnostic candidate genes identified by three machine algorithms. (F) Predicted nomograms of candidate genes for SCI diagnosis. To use it, locate the value for each biomarker (GPD1L, EPHX2, CYP1B1) on its respective scale and draw a line upward to the 'Points' axis to determine the score for each variable. Sum all the points to get the 'Total points'. (G) ROC curve of CYP1B1 in GSE151371 with an AUC value of 0.953. (H) ROC curve of EPHX2 in GSE151371 with an AUC value of 0.989. (I) ROC curve of GPD1L in GSE151371 with an AUC value of 0.957. (J) Visualization of SCI diagnostic candidate genes based on CTD pain inference scores. AUC, area under the curve; CTD, Comparative Toxicogenomics Database; CYP1B1, cytochrome P450 family 1 subfamily B member 1; EPHX2, epoxide hydrolase 2; GPD1L, glycerol-3-phosphate dehydrogenase 1-like; LASSO, least absolute shrinkage and selection operator; RMSE, root mean square error; ROC, receiver operating characteristic; SCI, spinal cord injury; SVM-RFE, support vector machine recursive feature elimination.

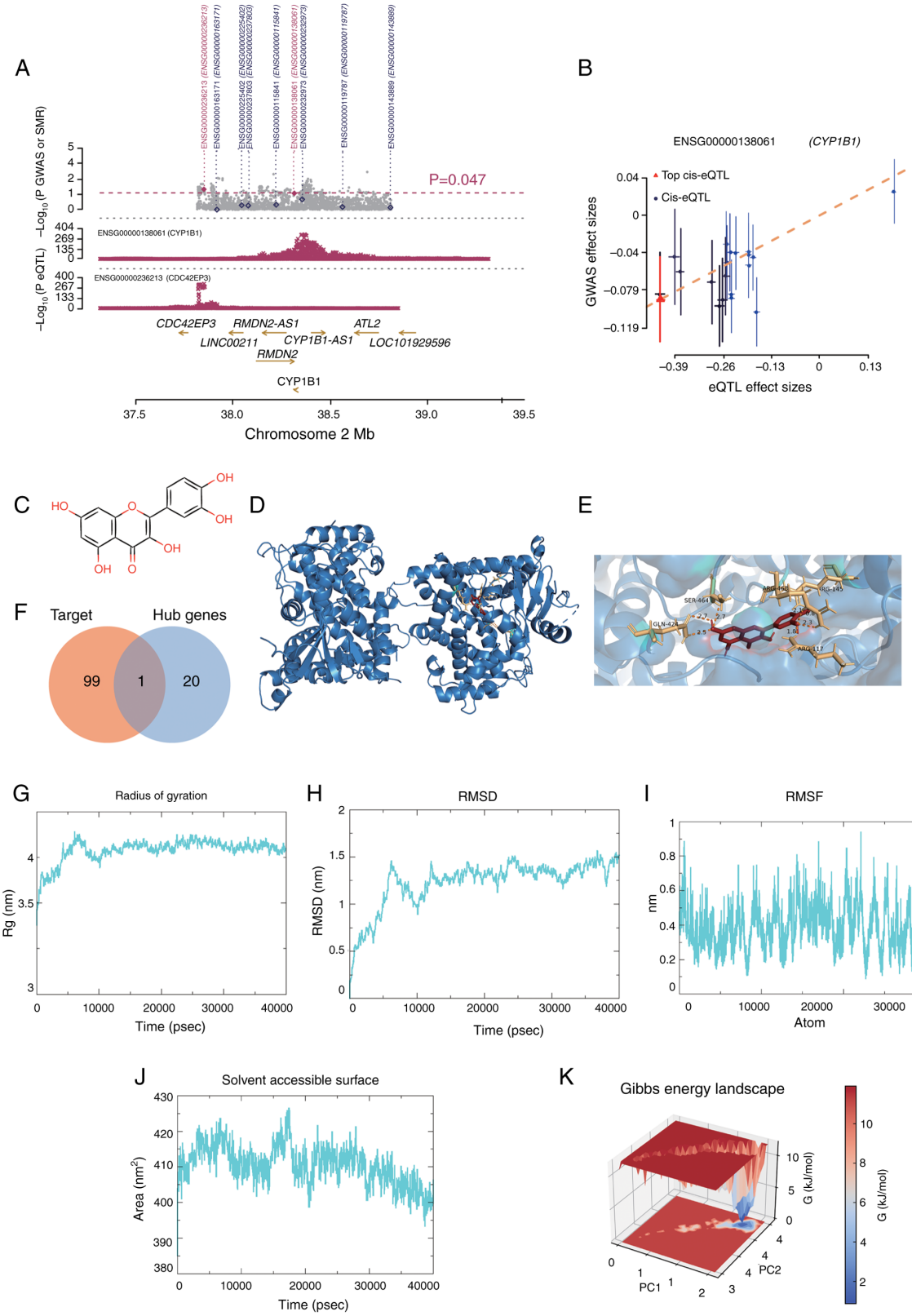

Figure 5. (A) MR association between CYP1B1 gene expression and trigeminal neuralgia in blood. All SNPs available in GWAS and eQTL data are shown in. (A) Grey dots represent the P-values of SNPs for GWAS, and diamonds represent P-values of probes for SMR tests. (B) P-values for eQTL analyses of CYP1B1 SNPs from GWAS (used in the heterogeneity in dependent instruments test) are plotted against effect sizes of SNPs from eQTL studies. The orange dashed line indicates the effect size estimate for the MR association at the top cis-eQTL. The error line is the standard error of the SNP effect. (C) Chemical structure of Que. (D) Interaction of the CYP1B1 receptor with Que ligands. The protein is depicted as a blue cartoon (α-helices and β-sheets) with its molecular surface shown in transparent gray. Que is shown as red sticks. (E) Detailed view of the local interactions within the Que-CYP1B1 binding pocket Protein residues are shown as blue sticks. The ligand, Que, is shown as red sticks. (F) Venn diagram of potential targets of Que and 21 core genes. (G) Rg of the Que-CYP1B1 complex. (H) RMSD of the Que-CYP1B1 complex. (I) RMSF of CYP1B1 protein residues. (J) Solvent accessible surface of the Que-CYP1B1 complex. (K) Free energy landscape of the Que-CYP1B1 complex. CYP1B1, cytochrome P450 family 1 subfamily B member 1; eQTL, expression-quantitative trait loci; GWAS, genome wide association study; MR, Mendelian randomization; PC, principal component; Que, quercetin; Rg, radius of gyration; RMSD, root mean square deviation; RMSF, root mean square fluctuation; SMR, summary-based Mendelian randomization.

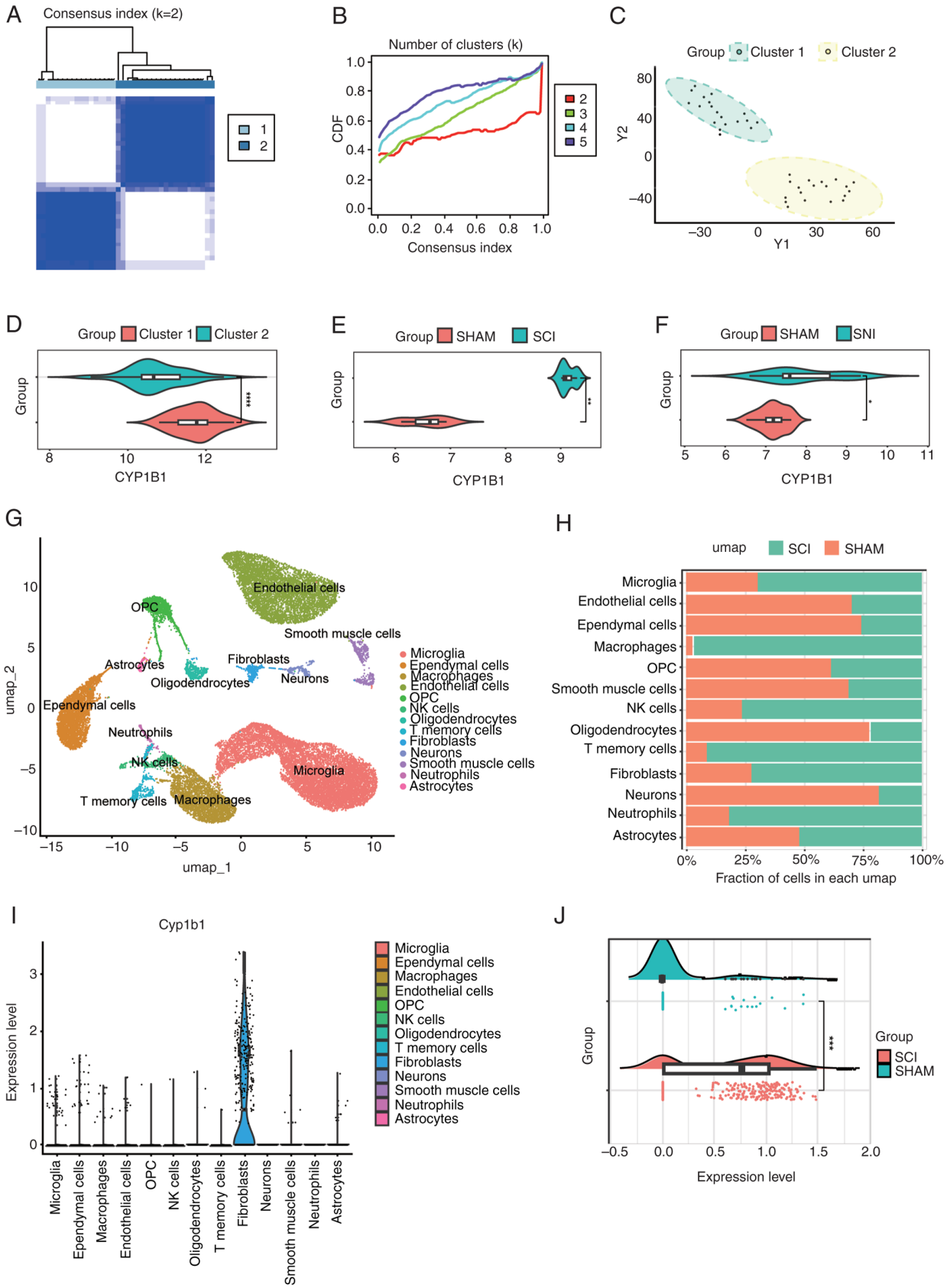

Figure 6. (A) A clustering heat map of the samples with the optimal clustering number set to k=2. (B) CDF curve for various values of k, constrained within the minimum range of the consensus index. (C) Principal component analysis graphs with the optimal clustering number set to k=2. (D) Differential expression of CYP1B1 across two distinct clusters. (E) CYP1B1 expression in the GSE171441 dataset. (F) CYP1B1 expression in the GSE236754 dataset. (G) A total of 13 cell populations were identified in the single-cell sequencing data from the GSE162610 dataset. (H) Proportion of the 13 cell populations in the two groups. (I) CYP1B1 expression in 13 cell populations. (J) Comparison of changes in CYP1B1 levels in fibroblasts of two groups. *P<0.05, **P<0.01, ***P<0.001 and ****P<0.0001. CDF, cumulative distribution function; CYP1B1, cytochrome P450 family 1 subfamily B member 1; NK, natural killer; OPC, oligodendrocyte precursor cells; SCI, spinal cord injury; SHAM, sham surgery group; umap, uniform manifold approximation and projection; Y1, Principal Component 1; Y2, Principal Component 2.

singular and smooth minimum energy cluster. In summary, the Que-CYP1B1 complex exhibited substantial binding stability, suggesting that Que effectively binds to CYP1B1.

CYP1B1 genotype identification and external validation. The NMF algorithm was utilized to cluster 38 SCI samples according to the expression profiles of genes associated with NP, as identified through the SMR approach. The clustering analysis exhibited optimal stability when the number of clusters, K, was designated as 2 (Fig. 6A). The cumulative distribution function curve exhibits fluctuations from 0.3 to 1.0 across the minimum range of the consensus index for varying values of K (Fig. 6B). Finally, the 38 SCI samples were classified into two subtypes: Cluster 1 (n=18) and cluster 2 (n=20). Principal component analysis demonstrated notable differences between cluster 1 and cluster 2 in the expression levels of NP-related genes (Fig. 6C). Furthermore, it was observed that the core gene CYP1B1 was highly expressed in the cluster 1 subtype (Fig. 6D). Validation using the GSE171441 and GSE236754 datasets demonstrated significant upregulation of CYP1B1 in both SCI and NP conditions compared with SHAM (Fig. 6E and F).

Single-cell sequencing analysis. In order to further study cellular infiltration following SCI and the expression of CYP1B1 in the affected cells, the single-cell GSE162610 dataset was analyzed, ensuring rigorous quality control and comprehensive analysis. In the processed ScSCI dataset, the cell populations were categorized into 13 distinct clusters (Fig. 6G). The alterations in the proportions of cells in the SCI group relative to the Con group were quantified (Fig. 6H). In this analysis, there was an observed increase in microglia, macrophages, natural killer cells, memory T cells, fibroblasts, neutrophils and astrocytes in the SCI group compared with that in the SHAM group. Conversely, there was a relative decrease in endothelial cells, ependymal cells, oligodendrocyte precursor cells, oligodendrocytes, smooth muscle cells and neurons. CYP1B1 exhibited elevated expression levels in fibroblasts compared with other cell types (Fig. 6I). Furthermore, compared with that in the SHAM group, the expression level of fibroblasts in the SCI group was significantly increased (Fig. 6J).

CYP1B1 expression is elevated in SCI and activated fibroblasts, with Que effectively inhibiting its expression. CYP1B1, identified as a prognostic biomarker through bioinformatics, MR and network pharmacology, and recognized as a therapeutic target for Que, requires further validation. Upon successful establishment of the SCI, SCI + Que and SHAM experimental models, spinal cord tissues were harvested on day 14 post-modeling. The detailed surgical protocol and tissue processing workflow are schematically illustrated in Fig. 7A. In comparison with the SHAM group, the SCI and SCI + Que group exhibited decreased MWT and TWLs on day 14 following surgery. Notably, the MWT and TWL values were significantly elevated in the SCI + Que group relative to the SCI group (Fig. 7B and C). The BMS scores of the Que-treated mice were superior to those of the SCI-treated mice by day 3 post-SCI surgery, with a statistically significant difference observed in BMS scores between the two groups at day 14 (Fig. 7D). These results suggest that Que may alleviate NP by increasing mechanical and thermal pain thresholds.

In the spinal cord tissues of the SCI group, both the protein and mRNA levels of CYP1B1 were markedly elevated compared with those in the SHAM group; however, treatment with Que significantly attenuated this expression (Fig. 7E-G). Furthermore, immunofluorescence analysis revealed a substantial increase in CYP1B1 expression within fibroblasts in the SCI group relative to the SHAM group, which was effectively reduced by Que treatment (Fig. 7H and I). *In vitro* experiments revealed a substantial elevation in CYP1B1 protein and mRNA levels in activated fibroblasts, which was subsequently attenuated by Que (Fig. 7J-L). Furthermore, fibroblasts exhibiting elevated CYP1B1 expression exhibited significant upregulation of Fn, and this expression was likewise inhibited by Que (Fig. 7M and N).

Discussion

In the present study, the SMR approach was utilized for the integrated analysis of GWAS summaries pertaining to NP, in conjunction with transcriptome sequencing data from public databases. The present multiomics investigation facilitated the synthesis of genomic and transcriptomic analyses. Specifically, genes associated with NP risk were identified by employing cis-eQTL gene variants as IVs and gene expression levels as exposure factors. Subsequently, transcriptome sequencing analysis was utilized to identify key modular genes associated with SCI, with the objective of elucidating the molecular mechanisms common to both SCI and NP. Furthermore, considering previous research that has demonstrated the beneficial effects of Que in the context of SCI and NP (60,61), network pharmacology approaches were incorporated to explore potential targets of Que among the core genes implicated in both conditions. The present study offers novel perspectives and identifies potential pathways for improving the diagnosis and treatment of NP associated with SCI. The mechanism investigated in this study is that when SCI occurs, neuropathic pain is associated with an increase in CYP1B1 expression in fibroblasts. Que alleviates neuropathic pain by inhibiting this upregulation of CYP1B1 (Fig. 8).

The management of NP poses a considerable clinical challenge. Despite previous advancements in elucidating the underlying mechanisms, such as disruptions in afferent pathways due to alterations in ion channels, elevated levels of spinal dynorphin, increased glutamate release from spinal primary afferent endings and the generation of ectopic action potentials, patients frequently do not receive sufficient analgesia in clinical practice (62,63). One etiological factor contributing to NP is SCI, which poses substantial challenges to clinical management when these conditions occur sequentially. The emergence of NP in individuals with SCI markedly exacerbates the deterioration of their quality of life (1,2). The present study primarily focused on NP following SCI. By comparison, conditions such as PHN and TN are classified as peripheral neuropathic pain. Although both PHN and TN are types of NP (1), the present research specifically aimed to investigate genes associated with NP in the context of SCI. Despite differences in etiology between peripheral and central neuropathic pain, both share common clinical features, including

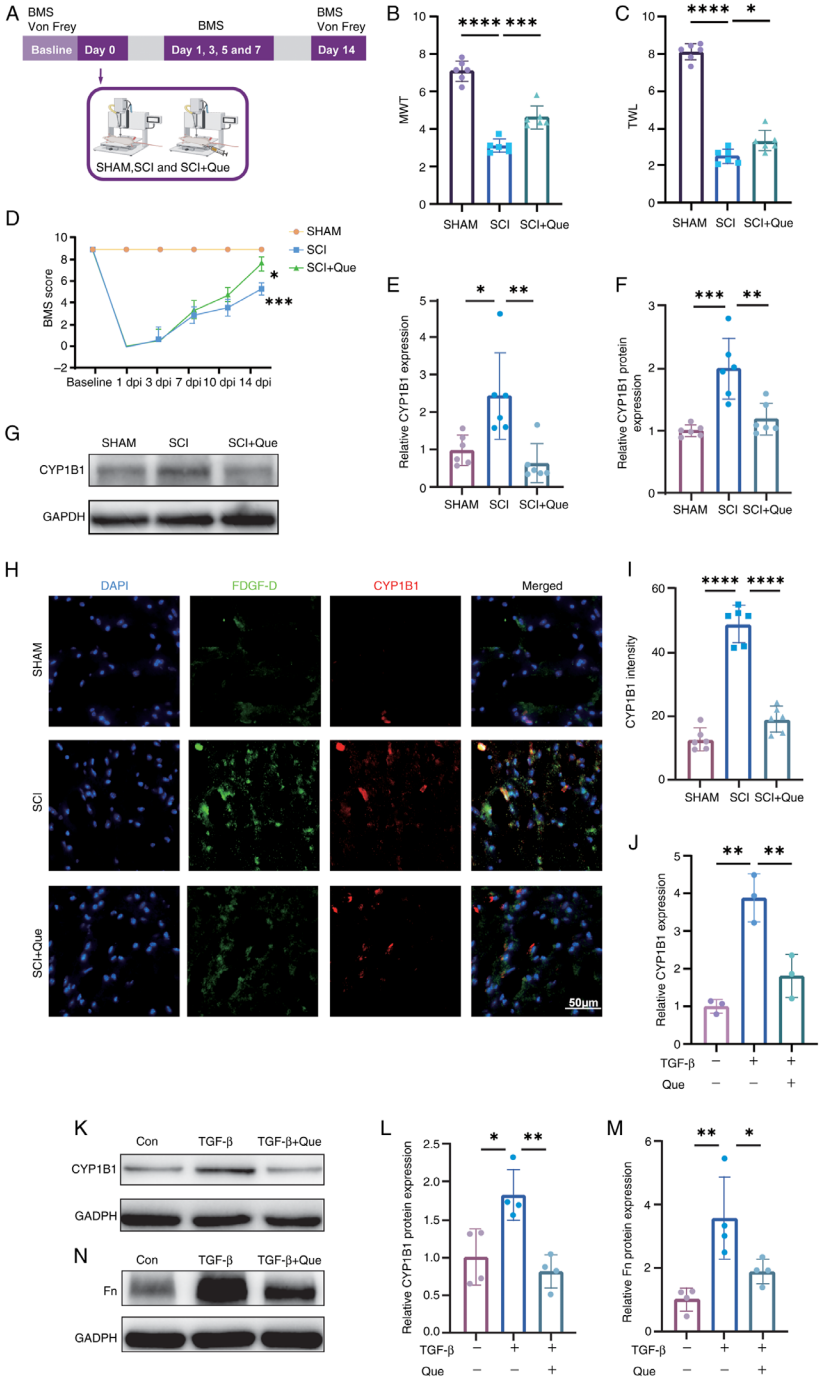

Figure 7. (A) Flow chart of the animal experiment. (B) MWT measurements for the SHAM, SCI and SCI + Que groups were recorded on day 14. (C) TWL for the SHAM, SCI and SCI + Que groups was also measured on day 14. (D) BMS scores for the SHAM, SCI and SCI + Que groups were assessed at baseline and on postoperative days 1, 3, 5, 7, 10 and 14. A statistically significant difference was observed (***P<0.001) between the SCI and SHAM groups of mice (n=6 each). Additionally, a significant difference was noted between the SCI and SCI + Que groups (*P<0.05), with n=6. (E) RT-qPCR assessment of CYP1B1 mRNA levels in spinal cord tissues from SHAM, SCI and SCI + Que groups, with expression levels normalized to GAPDH. (F) Semi-quantitative analysis of CYP1B1 protein levels in spinal cord tissues from the SHAM, SCI and SCI + Que groups, with fold-changes normalized to GAPDH. (G) Western blot analysis was conducted to assess CYP1B1 expression in spinal cord tissues from the SHAM, SCI and SCI + Que groups on day 14 post-modeling. (H) Immunofluorescence analysis was performed to assess the expression levels of CYP1B1 and the fibroblast marker PDGF-D in spinal cord tissues from the SHAM, SCI and SCI + Que groups, with n=6. Scale bar, 50 μm. (I) Quantitative fluorescence analysis of CYP1B1 expression was conducted on spinal cord tissues from the SHAM, SCI and SCI + Que groups. (J) RT-qPCR evaluation of CYP1B1 mRNA expression in fibroblasts treated under control conditions, with 10 ng/ml TGF-β and with 10 ng/ml TGF-β + 10 μmol/ml Que, with mRNA levels normalized to GAPDH. (K) Western blot analysis was performed to evaluate CYP1B1 expression in fibroblasts subjected to control conditions, 10 ng/ml TGF-β stimulation or co-treatment with 10 ng/ml TGF-β and 10 μmol/ml Que. (L) Semi-quantitative evaluation of CYP1B1 protein expression in fibroblasts subjected to control conditions, treated with 10 ng/ml TGF-β or treated with 10 ng/ml TGF-β combined with 10 μmol/ml Que, with protein levels normalized to GAPDH. (M) A semi-quantitative analysis was conducted on the Fn protein levels in fibroblasts subjected to control conditions, 10 ng/ml TGF-β treatment or treatment with a combination of 10 ng/ml TGF-β and 10 μmol/ml Que, with the resulting fold-changes normalized against GAPDH. (N) Western blot analysis was utilized to investigate Fn expression in fibroblasts under control conditions, after treatment with 10 ng/ml TGF-β or after co-treatment with 10 ng/ml TGF-β and 10 μmol/ml Que. The data are presented as the mean ± SEM, with sample sizes of n=6 per group for (B, C, D, E, F, G, H and I), n=3 per group for (J) and n=4 per group for (K, L, M and N). *P<0.05, **P<0.01, ***P<0.001 and ****P<0.0001. BMS, Basso Mouse Scale; Con, control; CYP1B1, cytochrome P450 family 1 subfamily B member 1; PDGF-D, platelet-derived growth factor D ;dpi, days post-injury; Fn, Fibronectin; MWT, mechanical withdrawal threshold; Que, quercetin; RT-qPCR, reverse transcription-quantitative PCR; SCI, spinal cord injury; SHAM, sham surgery group; TWL, thermal withdrawal latency.

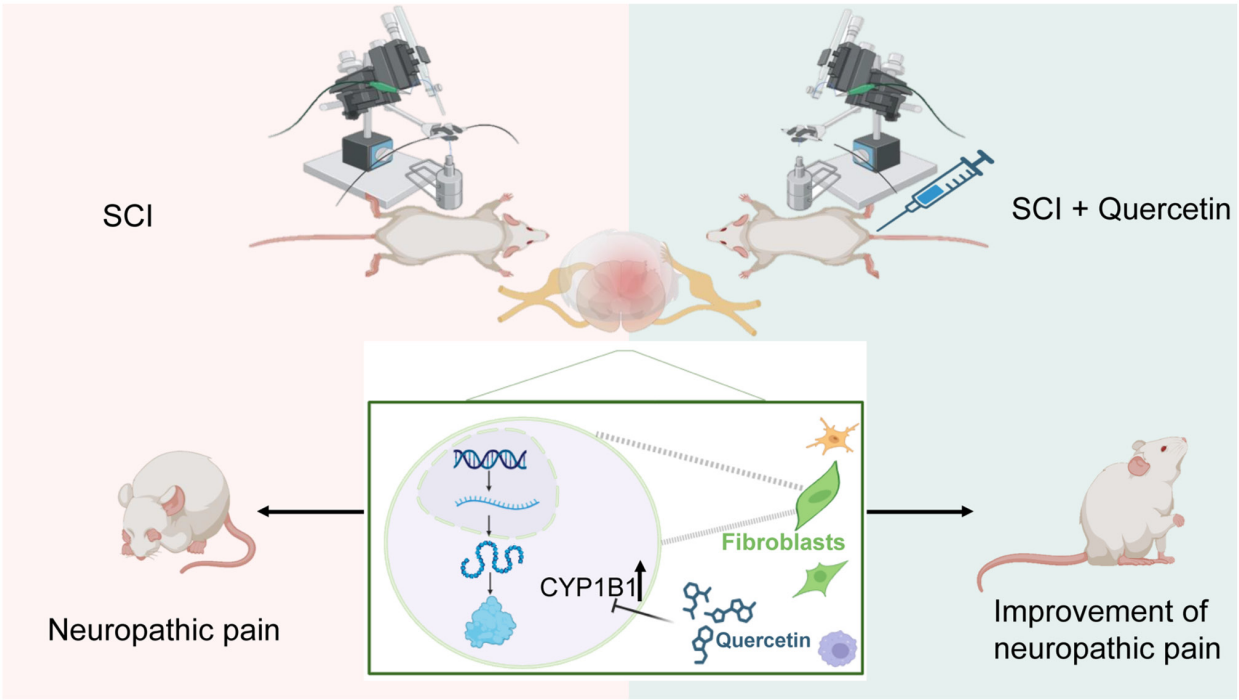

Figure 8. Mechanism diagram. CYP1B1, cytochrome P450 family 1 subfamily B member 1; SCI, spinal cord injury.

hyperalgesia and allodynia (63). An SCI mouse model was employed in the present study. The principal goals were to elucidate the mechanisms underlying NP after SCI and to identify effective therapeutic strategies, particularly to determine whether the specific intervention alleviated NP-related symptoms such as hyperalgesia and allodynia. Furthermore, both peripheral NP and central NP share a variety of interconnected cellular and molecular mechanisms, particularly through interactions among neuroglial cells and the involvement of neuroinflammatory signaling. While peripheral NP, exemplified by PHN or TN, and central neuropathic pain, such as that resulting from SCI, originate from distinct injury sites, they ultimately engage similar pathways that culminate in hyperexcitability, sensitization and the chronicity of pain. A significant mechanism underlying these processes is the activation of neuroglial cells. Following peripheral nerve damage, satellite glial cells within the dorsal root ganglia become activated. These glial cells secrete pro-inflammatory cytokines, including tumor necrosis factor-α, interleukin-1β (IL-1β) and adenosine triphosphate, which enhance neuronal excitability and promote peripheral sensitization. In parallel, SCI induces the activation of microglia and astrocytes in the central nervous system. Activated microglia release brain-derived neurotrophic factor and various cytokines, which disrupt inhibitory mechanisms and facilitate excitatory signaling. Meanwhile, astrocytes play a crucial role in sustaining a neuroinflammatory response, thereby contributing to the ongoing central sensitization (64,65). TN and PHN represent classical models of NP characterized by distinct clinical phenotypes. A key aim of the present study was to investigate the shared molecular networks associated with NP, rather than narrowing the focus to specific etiological subtypes. Previous studies have infrequently explored the molecular mechanisms and pathways within the context of these two interrelated diseases concurrently. By treating these conditions as distinct yet interconnected entities and analyzing them collectively, a deeper and more holistic understanding of the underlying molecular mechanisms and pathways can be achieved. The simultaneous consideration of these conditions enables a more profound insight into the progression of NP, from its initial onset to its manifestation following SCI.

The onset of NP following SCI is markedly associated with the recruitment and activation of a substantial number of immune cells, predominantly from the innate immune system. The inflammation accompanying NP and SCI constitutes a complex process involving various cell types and a diverse array of inflammatory cytokines that interact synergistically (66,67). While the immune response possesses the ability to modulate inflammation and mitigate its persistence, it may also facilitate the transition from acute to chronic pain. Empirical evidence suggests that the immune response serves a notable role in sustaining persistent pain, with considerable infiltration of immune cells acting as a primary catalyst for neurodegeneration subsequent to SCI (68,69).

Inflammation is an adaptive physiological process that facilitates tissue healing and regeneration. However, if neuroinflammatory responses persist after the resolution of the initial inflammatory event, this may lead to the development of chronic pain (70). The involvement of fibroblasts in NP following SCI has been investigated, with a focus on their roles in scar formation, extracellular matrix remodeling and the secretion of pro-inflammatory cytokines and chemokines. Fibrotic scars are also observed following SCI (71,72). Research indicates that TGF-β serves a crucial role in promoting the expression of collagen (73), a recognized marker of fibroblast activation (74). Consequently, in order to replicate the unique environment associated with SCI *in vivo*, the present study employed TGF-β to conduct a functional validation analysis

aimed at assessing fibroblast activation. Furthermore, the interactions among fibroblasts, immune cells and neurons have been acknowledged as potential factors influencing the development and progression of NP post-SCI (75,76). Research indicates that Fn is predominantly synthesized and secreted by fibroblasts, serving a crucial function as an extracellular matrix protein. The presence of Fn within neurons has the potential to modify neuronal growth and signal transmission. Furthermore, Fn engages with cell surface receptors, including integrins, to modulate the expression of genes associated with pain. This interaction may facilitate inflammation and enhance the sensitivity of nerve endings, thereby amplifying pain responses (77,78).

CYP1B1 is an important enzyme involved in the metabolism of a wide range of endogenous and exogenous substances (79). Its role in NP following SCI includes modulating the inflammatory response and regulating oxidative stress levels. CYP1B1 functions as a regulator of reactive oxygen species (ROS) (80), facilitating the *in vitro* metabolism of arachidonic acid into various metabolites, including 20-hydroxy-eicosatetraenoic acid, which subsequently stimulates nicotinamide-adenine dinucleotide phosphate oxidase activity and promotes ROS generation (81). In the context of brain tissue, testosterone can induce hypertension and neuroinflammation through its CYP1B1-derived metabolite, 6β-hydroxytestosterone (82). The present investigation revealed altered expression levels of CYP1B1 following SCI, with single-cell analysis pinpointing its localization within fibroblasts, thereby indicating a potential involvement of CYP1B1 in SCI mechanisms. Nevertheless, the specific role of CYP1B1 in fibroblasts concerning the onset and progression of NP following SCI remains to be elucidated. In light of these observations, the present study suggested that the abnormal activation of fibroblasts and CYP1B1 subsequent to SCI markedly contributes to the progression of NP, primarily through the activation of ROS and inflammation, which are key contributors to neuronal cell injury and death post-SCI (83).

Current clinical strategies for managing NP post-SCI encompass pharmacological options such as antiepileptic, antidepressant and opioid medications, alongside non-pharmacological conditioning techniques, including spinal cord electrical stimulation, TMS and tDCS (7,8). However, the mechanisms driving the onset and progression of NP following SCI remain inadequately elucidated. The majority of available drugs primarily address symptomatic relief, with limited capacity for targeting specific underlying mechanisms; consequently, there exists a considerable gap in effective treatments aimed at ameliorating NP following SCI (84). Studies suggest that inhibiting CYP1B1 activity can reduce the production of ROS, subsequently decreasing oxidative stress-induced neuronal damage and alleviating NP following SCI (85,86).

Numerous natural compounds exhibit neuroprotective and anti-inflammatory properties, with notable examples including resveratrol, curcumin and Que (19,87,88). In molecular docking experiments, paracetamol, aspirin and caffeine served as negative control agents. Beyond its neuroprotective and anti-inflammatory capabilities, Que is also acknowledged for its antioxidant properties. Research indicates that Que can markedly enhance the total antioxidant status in both plasma and spinal cord tissue following SCI, thereby highlighting its potential therapeutic role for this ailment (89). Que is recognized for its anti-inflammatory and antioxidant properties, with research suggesting its therapeutic potential for both general inflammation and SCI. Que also modulates neuronal receptors, including T-type calcium channels and cyclooxygenase-2, thereby contributing to the reduction of central sensitization and the alleviation of hyperalgesia (90). Furthermore, it inhibits the expression of inflammatory cytokines such as tumor necrosis factor-α and IL-1β, thereby mitigating inflammation-associated neuronal damage (91). Its antioxidative properties facilitate the clearance of free radicals, consequently reducing oxidative stress levels (92). Consequently, the present research revealed that CYP1B1 not only serves as a biomarker for NP following SCI, but it was also recognized as a potential target of Que in receptor prediction analysis. This observation implies that Que might mitigate oxidative stress through the inhibition of CYP1B1, thereby providing a theoretical foundation for further exploration of the role of CYP1B1 in NP following SCI and enhancing the understanding of the underlying mechanisms involved in NP management after SCI. Nevertheless, the precise molecular pathways through which Que inhibits CYP1B1-mediated NP necessitate additional research.

The analysis in the present study predominantly focused on the mouse SCI dataset (GSE171441) during the subacute phase, specifically at 14 days post-injury. Correspondingly, animal experiments were performed utilizing a 14-day SCI model for both model establishment and experimental validation. This emphasis on the subacute phase is justified, as oxidative stress is intricately linked to disease progression, and CYP1B1, recognized as a biomarker for post-SCI NP, functions as a regulator of ROS (80). Furthermore, oxidative stress is acknowledged as a distinguishing feature of the subacute phase following SCI. Thus, the results of the present study suggested that oxidative stress is an important factor in the pathogenesis of post-SCI NP and that attenuation of oxidative stress during this subacute phase could serve as an effective therapeutic approach (93). Building on this premise, the 14-day SCI animal model was employed to investigate the relevant mechanisms and assess the therapeutic potential of Que intervention. Additional research is warranted to explore the mechanisms and associated pharmacological interventions throughout the chronic phase following the onset and progression of NP subsequent to SCI.

The present study has a number of limitations. First, the availability of high-quality human datasets pertaining to NP after SCI is limited and displays considerable variability. Drawing on the present findings related to conditions such as PHN and TN, the shared characteristics of NP were examined and a novel strategy for managing NP after SCI was introduced. Nonetheless, additional efforts in accumulating datasets specific to NP after SCI are required for a deeper understanding of the underlying mechanisms driving the onset and progression of this condition. Second, the present investigation primarily concentrated on elucidating and validating the mechanisms and pharmacological interventions for NP after SCI during the subacute phase. It is important to further examine the molecular mechanisms and therapeutic interventions relevant to other stages, including the acute

and chronic phases. Additionally, the significance of the core biomarker CYP1B1 and the influence of Que during these distinct phases warrant further inquiry and confirmation. Third, the present study investigated the therapeutic effect of Que at a dose of 7.5 mg/kg twice daily. However, the effects of other doses were not examined. Future studies will evaluate multiple doses of Que to determine the optimal therapeutic range, providing a theoretical basis for its clinical application. Fourth, in single-cell analysis, no further distinction was made between myofibroblasts or resting fibroblasts, and in future studies, more single-cell sequencing datasets should be obtained for comprehensive analysis of fibroblast subsets. Fifth, in the *in vitro* component of the present study, the established fibroblast activator TGF-β was primarily utilized, and the role of CYP1B1 in fibroblast responses to other NP-associated stimuli, such as lipopolysaccharide and H_2O_2, requires further investigation. In summary, this integrated multi-omics and experimental study identifies CYP1B1 as a key mediator of neuropathic pain (NP) following spinal cord injury, specifically highlighting its role in fibroblast activation and associated neuroinflammatory and oxidative pathways. We demonstrate that quercetin exerts analgesic effects, at least in part, by inhibiting CYP1B1, providing a mechanistic basis for its neuroprotective properties. Moreover, these findings not only advance our understanding of central NP pathogenesis but also support the therapeutic targeting of CYP1B1, thereby opening new translational avenues for developing treatments for neuropathic pain after SCI.

Acknowledgements

Not applicable.

Funding

Funding was obtained from the Natural Science Foundation of Guangdong Province (grant no. 2514050000156), the Research Project of Guangdong Bureau of Traditional Chinese Medicine (grant no. 20251251), the Special Fund for Clinical Scientific Research of Guangdong Medical Association (grant no. 2024HY-B4001), the Norman Bethune Foundation Enzer Pain Management Medical Research Program (grant no. ezmr2023-080), the Education, Teaching and Research Project of The Third Affiliated Hospital of The Southern Medical University (grant no. JXY202408), and the Youth Fund Program of Hainan Provincial Natural Science Foundation of China (grant no. 822QN451).

Availability of data and materials

The data generated in the present study may be requested from the corresponding author.

Authors' contributions

PZ contributed to the conceptualization, methodology and data curation of the study. PZ, LL, YC, JiaC, CC , XZ, JiuC, YD, PS and JZ were responsible for data analysis and interpretation. PZ, LL, YC, JiaC, ZL, YL, SW, ST, WZ and CC were responsible for the animal and cell experiments. XZ, JiuC and YD were responsible for acquiring resources and validation. PZ, ZL and YL provided administrative oversight. SW, ST and WZ acquired the funding. PS and JZ supervised the project. PZ, PS and JZ contributed to the writing, reviewing and editing of the final manuscript. PZ, LL and YC confirm the authenticity of all the raw data. All authors have read and approved the final version of the manuscript.

Ethics approval and consent to participate

All experimental procedures involving animals were carried out in strict accordance with the guidelines for the care and use of laboratory animals and were approved by the Institutional Animal Care and Use Committee of Daoke Pharmaceutical Technology (Guangdong) Co., Ltd. (Guangzhou, China; approval no. IACUC-DK-2024-04-10-01).

Patient consent for publication

Not applicable.

Competing interests

The authors declare that they have no competing interests.

References

1. Finnerup NB, Kuner R and Jensen TS: Neuropathic Pain: From mechanisms to treatment. Physiol Rev 101: 259-301, 2021.
2. Burke D, Fullen BM, Stokes D and Lennon O: Neuropathic pain prevalence following spinal cord injury: A systematic review and meta-analysis. Eur J Pain 21: 29-44, 2017.
3. Hergenroeder GW, Redell JB, Choi HA, Schmitt L, Donovan W, Francisco GE, Schmitt K, Moore AN and Dash PK: Increased levels of circulating glial fibrillary acidic protein and collapsin response mediator Protein-2 autoantibodies in the acute stage of spinal cord injury predict the subsequent development of neuropathic pain. J Neurotraum 35: 2530-2539, 2018.
4. Widerström-Noga E: Neuropathic pain and spinal cord injury: Phenotypes and pharmacological management. Drugs 77: 967-984, 2017.
5. Orr MB and Gensel JC: Spinal cord injury scarring and inflammation: Therapies targeting glial and inflammatory responses. Neurotherapeutics 15: 541-553, 2018.
6. O'Shea TM, Burda JE and Sofroniew MV: Cell biology of spinal cord injury and repair. J Clin Invest 127: 3259-3270, 2017.
7. Boldt I, Eriks-Hoogland I, Brinkhof MW, de Bie R, Joggi D and von Elm E: Non-pharmacological interventions for chronic pain in people with spinal cord injury. Cochrane Database Syst Rev 2014: CD009177, 2014.
8. Mehta S, McIntyre A, Janzen S, Loh E and Teasell R; Spinal Cord Injury Rehabilitation Evidence Team: Systematic review of pharmacologic treatments of pain after spinal cord injury: An update. Arch Phys Med Rehabil 97: 1381-1391.e1, 2016.
9. Loh E, Mirkowski M, Agudelo AR, Allison DJ, Benton B, Bryce TN, Guilcher S, Jeji T, Kras-Dupuis A, Kreutzwiser D, *et al*: The CanPain SCI clinical practice guidelines for rehabilitation management of neuropathic pain after spinal cord injury: 2021 update. Spinal Cord 60: 548-566, 2022.
10. Liu C, Liu DQ, Tian YK, Mei W, Tian XB, Xu AJ and Zhou YQ: The emerging role of quercetin in the treatment of chronic pain. Curr Neuropharmacol 20: 2346-2353, 2022.
11. Yang H, Yang T, Heng C, Zhou Y, Jiang Z, Qian X, Du L, Mao S, Yin X and Lu Q: Quercetin improves nonalcoholic fatty liver by ameliorating inflammation, oxidative stress, and lipid metabolism in db/db mice. Phytother Res 33: 3140-3152, 2019.
12. Gao W, Zan Y, Wang ZJ, Hu XY and Huang F: Quercetin ameliorates paclitaxel-induced neuropathic pain by stabilizing mast cells, and subsequently blocking PKCε-dependent activation of TRPV1. Acta Pharmacol Sin 37: 1166-1177, 2016.

13. Wang R, Qiu Z, Wang G, Hu Q, Shi N, Zhang Z, Wu Y and Zhou C: Quercetin attenuates diabetic neuropathic pain by inhibiting mTOR/p70S6K pathway-mediated changes of synaptic morphology and synaptic protein levels in spinal dorsal horn of db/db mice. Eur J Pharmacol 882: 173266, 2020.
14. Abbey EL and Rankin JW: Effect of quercetin supplementation on repeated-sprint performance, xanthine oxidase activity, and inflammation. Int J Sport Nutr Exerc Metab 21: 91-96, 2011.
15. Zhao L, Wang H and Du X: The therapeutic use of quercetin in ophthalmology: Recent applications. Biomed Pharmacother 137: 111371, 2021.
16. Li Y, Yao J, Han C, Yang J, Chaudhry MT, Wang S, Liu H and Yin Y: Quercetin, inflammation and immunity. Nutrients 8: 167, 2016.
17. Costa LG, Garrick JM, Roquè PJ and Pellacani C: Mechanisms of neuroprotection by Quercetin: Counteracting oxidative stress and more. Oxid Med Cell Longev 2016: 2986796, 2016.
18. Shao Z, Wang B, Shi Y, Xie C, Huang C, Chen B, Zhang H, Zeng G, Liang H, Wu Y, *et al*: Senolytic agent Quercetin ameliorates intervertebral disc degeneration via the Nrf2/NF-κB axis. Osteoarthritis Cartilage 29: 413-422, 2021.
19. Chiang MC, Tsai TY and Wang CJ: The potential benefits of quercetin for brain health: A review of Anti-inflammatory and neuroprotective mechanisms. Int J Mol Sci 24: 6328, 2023.
20. Grewal AK, Singh TG, Sharma D, Sharma V, Singh M, Rahman MH, Najda A, Walasek-Janusz M, Kamel M, Albadrani GM, *et al*: Mechanistic insights and perspectives involved in neuroprotective action of quercetin. Biomed Pharmacother 140: 111729, 2021.
21. Elsworth B, Lyon B, Alexander T, Liu Y, Matthews P, Hallett J, Bates P, Palmer T, Haberland V, Smith GD, *et al*: The MRC IEU OpenGWAS data infrastructure. bioRxiv: August 10, 2020 doi: 10.1101/2020.08.10.244293.
22. Kurki MI, Karjalainen J, Palta P, Sipilä TP, Kristiansson K, Donner KM, Reeve MP, Laivuori H, Aavikko M, Kaunisto MA, *et al*: FinnGen provides genetic insights from a well-phenotyped isolated population. Nature 613: 508-518, 2023.
23. Võsa U, Claringbould A, Westra HJ, Bonder MJ, Deelen P, Zeng B, Kirsten H, Saha A, Kreuzhuber R, Yazar S, *et al*: Large-scale cis- and trans-eQTL analyses identify thousands of genetic loci and polygenic scores that regulate blood gene expression. Nat Genet 53: 1300-1310, 2021.
24. Kyritsis N, Torres-Espín A, Schupp PG, Huie JR, Chou A, Duong-Fernandez X, Thomas LH, Tsolinas RE, Hemmerle DD, Pascual LU, *et al*: Diagnostic blood RNA profiles for human acute spinal cord injury. J Exp Med 218: e20201795, 2021.
25. Milich LM, Choi JS, Ryan C, Cerqueira SR, Benavides S, Yahn SL, Tsoulfas P and Lee JK: Single-cell analysis of the cellular heterogeneity and interactions in the injured mouse spinal cord. J Exp Med 218: e20210040, 2021.
26. Patel M, Li Y, Anderson J, Castro-Pedrido S, Skinner R, Lei S, Finkel Z, Rodriguez B, Esteban F, Lee KB, *et al*: Gsx1 promotes locomotor functional recovery after spinal cord injury. Mol Ther 29: 2469-2482, 2021.
27. Ghazisaeidi S, Muley MM, Tu Y, Finn DP, Kolahdouzan M, Pitcher GM, Kim D, Sengar AS, Ramani AK, Brudno M and Salter MW: Conserved transcriptional programming across sex and species after peripheral nerve injury predicts treatments for neuropathic pain. Br J Pharmacol 180: 2822-2836, 2023.
28. Zhu Z, Zhang F, Hu H, Bakshi A, Robinson MR, Powell JE, Montgomery GW, Goddard ME, Wray NR, Visscher PM and Yang J: Integration of summary data from GWAS and eQTL studies predicts complex trait gene targets. Nat Genet May 48: 481-487, 2016.
29. Langfelder P and Horvath S: WGCNA: An R package for weighted correlation network analysis. BMC Bioinformatics 9: 559, 2008.
30. Bardou P, Mariette J, Escudié F, Djemiel C and Klopp C: Jvenn: An interactive Venn diagram viewer. BMC Bioinformatics 15: 293, 2014.
31. The Gene Ontology Consortium: The Gene Ontology Resource: 20 years and still GOing strong. Nucleic Acids Res 47: D330-D338, 2019.
32. Ogata H, Goto S, Sato K, Fujibuchi W, Bono H and Kanehisa M: KEGG: Kyoto encyclopedia of genes and genomes. Nucleic Acids Res 27: 29-34, 1999.
33. Li J, Miao B, Wang S, Dong W, Xu H, Si C, Wang W, Duan S, Lou J, Bao Z, *et al*: Hiplot: A comprehensive and easy-to-use web service for boosting publication-ready biomedical data visualization. Brief Bioinform 23: bbac261, 2022.
34. Szklarczyk D, Gable AL, Nastou KC, Lyon D, Kirsch R, Pyysalo S, Doncheva NT, Legeay M, Fang T, Bork P, *et al*: The STRING database in 2021: Customizable protein-protein Networks, and functional characterization of user-uploaded gene/measurement sets. Nucleic Acids Res 49: D605-D601, 20212.
35. Shannon P, Markiel A, Ozier O, Baliga NS, Wang JT, Ramage D, Amin N, Schwikowski B and Ideker T: Cytoscape: A software environment for integrated models of biomolecular interaction networks. Genome Res 13: 2498-2504, 2003.
36. Bindea G, Mlecnik B, Tosolini M, Kirilovsky A, Waldner M, Obenauf AC, Angell H, Fredriksen T, Lafontaine L, Berger A, *et al*: Spatiotemporal dynamics of intratumoral immune cells reveal the immune landscape in human cancer. Immunity 39: 782-795, 2013.
37. Barbie DA, Tamayo P, Boehm JS, Kim SY, Moody SE, Dunn IF, Schinzel AC, Sandy P, Meylan E, Scholl C, *et al*: Systematic RNA interference reveals that oncogenic KRAS-driven cancers require TBK1. Nature 462: 108-112, 2009.
38. Yang C, Delcher C, Shenkman E and Ranka S: Machine learning approaches for predicting high cost high need patient expenditures in health care. Biomed Eng Online 17 (Suppl 1): S131, 2018.
39. Sahran S, Albashish D, Abdullah A, Shukor NA, Hayati Md and Pauzi S: Absolute cosine-based SVM-RFE feature selection method for prostate histopathological grading. Artif Intell Med 87: 78-90, 2018.
40. Degenhardt F, Seifert S and Szymczak S: Evaluation of variable selection methods for random forests and omics data sets. Brief Bioinform 20: 492-503, 2019.
41. Friedman J, Hastie T and Tibshirani R: Regularization paths for generalized linear models via coordinate descent. J Stat Softw 33: 1-22, 2010.
42. Alderden J, Pepper GA, Wilson A, Whitney JD, Richardson S, Butcher R, Jo Y and Cummins MR: Predicting pressure injury in critical care patients: A Machine-learning model. Am J Crit Care 27: 461-468, 2018.
43. Yoon S and Kim S: AdaBoost-based multiple SVM-RFE for classification of mammograms in DDSM. BMC Med Inform Decis Mak 9 (Suppl 1): S1, 2009.
44. Ding X, Qin J, Huang F, Feng F and Luo L: The combination of machine learning and untargeted metabolomics identifies the lipid metabolism-related gene CH25H as a potential biomarker in asthma. Inflamm Res 72: 1099-1119, 2023.
45. Li Y and Song M: Exact Model-free function inference using uniform marginal counts for null population. Bioinformatics 41: btaf121, 2025.
46. Robin X, Turck N, Hainard A, Tiberti N, Lisacek F, Sanchez JC and Müller M: pROC: An open-source package for R and S+ to analyze and compare ROC curves. BMC Bioinformatics 12: 77, 2011.
47. Daina A, Michielin O and Zoete V: SwissTargetPrediction: Updated data and new features for efficient prediction of protein targets of small molecules. Nucleic Acids Res 47: W357-W364, 2019.
48. Forli S, Huey R, Pique ME, Sanner MF, Goodsell DS and Olson AJ: Computational Protein-ligand docking and virtual drug screening with the AutoDock suite. Nat Protoc 11: 905-919, 2016.
49. Trott O and Olson AJ: AutoDock Vina: Improving the speed and accuracy of docking with a new scoring function, efficient optimization, and multithreading. J Comput Chem 31: 455-461, 2010.
50. DeLano WL: Unraveling hot spots in binding interfaces: Progress and challenges. Curr Opin Struct Biol 12: 14-20, 2002.
51. Hao Y, Hao S, Andersen-Nissen E, Mauck WM III, Zheng S, Butler A, Lee MJ, Wilk AJ, Darby C, Zager M, *et al*: Integrated analysis of multimodal single-cell data. Cell 184: 3573-3587.e29, 2021.
52. Butler A, Hoffman P, Smibert P, Papalexi E and Satija R: Integrating single-cell transcriptomic data across different conditions, technologies, and species. Nat Biotechnol 36: 411-420, 2018.
53. Valenzi E, Bulik M, Tabib T, Morse C, Sembrat J, Trejo Bittar H, Rojas M and Lafyatis R: Single-cell analysis reveals fibroblast heterogeneity and myofibroblasts in systemic sclerosis-associated interstitial lung disease. Ann Rheum Dis 78: 1379-1387, 2019.
54. Franzén O, Gan LM and Björkegren JLM: PanglaoDB: A web server for exploration of mouse and human single-cell RNA sequencing data. Database (Oxford) 2019: baz046, 2019.
55. Zhang X, Lan Y, Xu J, Quan F, Zhao E, Deng C, Luo T, Xu L, Liao G, Yan M, *et al*: CellMarker: A manually curated resource of cell markers in human and mouse. Nucleic Acids Res 47: D721-D728, 2019.

56. Anjaneyulu M and Chopra K: Quercetin, a bioflavonoid, attenuates thermal hyperalgesia in a mouse model of diabetic neuropathic pain. Prog Neuropsychopharmacol Biol Psychiatry 27: 1001-1005, 2003.
57. Fan H, Tang HB, Shan LQ, Liu SC, Huang DG, Chen X, Chen Z, Yang M, Yin XH, Yang H and Hao DJ: Quercetin prevents necroptosis of oligodendrocytes by inhibiting macrophages/microglia polarization to M1 phenotype after spinal cord injury in rats. J Neuroinflammation 16: 206, 2019.
58. Basso DM, Fisher LC, Anderson AJ, Jakeman LB, McTigue DM and Popovich PG: Basso mouse scale for locomotion detects differences in recovery after spinal cord injury in five common mouse strains. J Neurotrauma 23: 635-659, 2006.
59. Livak KJ and Schmittgen TD: Analysis of relative gene expression data using Real-time quantitative PCR and the 2(-Delta Delta C(T)) method. Methods 25: 402-408, 2001.
60. Wang X, Fu Y, Botchway BOA, Zhang Y, Zhang Y, Jin T and Liu X: Quercetin can improve spinal cord injury by regulating the mTOR signaling pathway. Front Neurol 13: 905640, 2022.
61. Bannister K, Sachau J, Baron R and Dickenson AH: Neuropathic Pain: Mechanism-based therapeutics. Annu Rev Pharmacol Toxicol 60: 257-274, 2020.
62. Torrance N, Ferguson JA, Afolabi E, Bennett MI, Serpell MG, Dunn KM and Smith BH: Neuropathic pain in the community: More under-treated than refractory? Pain 154: 690-699, 2013.
63. Jensen TS and Finnerup NB: Allodynia and hyperalgesia in neuropathic pain: Clinical manifestations and mechanisms. Lancet Neurol 13: 924-935, 2014.
64. Szok D, Tajti J, Nyári A and Vécsei L: Therapeutic approaches for peripheral and central neuropathic pain. Behav Neurol 2019: 8685954, 2019.
65. McGinnis A and Ji RR: The similar and distinct roles of satellite glial cells and spinal astrocytes in neuropathic pain. Cells 12: 965, 2023.
66. Calvo M, Dawes JM and Bennett DL: The role of the immune system in the generation of neuropathic pain. Lancet Neurol 11: 629-642, 2012.
67. Hellenbrand DJ, Quinn CM, Piper ZJ, Morehouse CN, Fixel JA and Hanna AS: Inflammation after spinal cord injury: A review of the critical timeline of signaling cues and cellular infiltration. J Neuroinflammation 18: 284, 2021.
68. Glaser J, Gonzalez R, Perreau VM, Cotman CW and Keirstead HS: Neutralization of the chemokine CXCL10 enhances tissue sparing and angiogenesis following spinal cord injury. J Neurosci Res 77: 701-708, 2004.
69. Garcia E, Aguilar-Cevallos J, Silva-Garcia R and Ibarra A: Cytokine and growth factor activation in vivo and in vitro after spinal cord injury. Mediators Inflamm 2016: 9476020, 2016.
70. Sommer C, Leinders M and Üçeyler N: Inflammation in the pathophysiology of neuropathic pain. Pain 159: 595-602, 2018.
71. Tang L, Song Z, Wang J, He S and Liu C: Regulatory role of neuronal guidance proteins in spinal cord injury. Neural Regen Res: May 6, 2025 (Epub ahead of print). doi: 10.4103/NRR.NRR-D-24-00564.
72. Neshasteh-Riz A, Ramezani F, Kookli K, Moghaddas Fazeli S, Motamed A, Nasirinezhad F, Janzadeh A, Hamblin MR and Asadi M: Optimization of the duration and dose of photobiomodulation therapy (660 nm Laser) for spinal cord injury in rats. Photobiomodul Photomed Laser Surg 40: 488-498, 2022.
73. Huang Y, Gao P, Qin T, Chu B, Xu T, Yi J, Wang Q, Yang Z, Jiang T, Fan J, *et al*: Delayed inhibition of collagen deposition by targeting bone morphogenetic protein 1 promotes recovery after spinal cord injury. Matrix Biol 118: 69-91, 2023.
74. Frangogiannis N: Transforming growth factor-β in tissue fibrosis. J Exp Med 217: e20190103, 2020.
75. Zhou X, He X and Ren Y: Function of microglia and macrophages in secondary damage after spinal cord injury. Neural Regen Res 9: 1787-1795, 2014.
76. Ji RR, Xu ZZ and Gao YJ: Emerging targets in neuroinflammation-driven chronic pain. Nat Rev Drug Discov 13: 533-548, 2014.
77. Schoch HJ, Fischer S and Marti HH: Hypoxia-induced vascular endothelial growth factor expression causes vascular leakage in the brain. Brain 125: 2549-2557, 2002.
78. Dina OA, Parada CA, Yeh J, Chen X, McCarter GC and Levine JD: Integrin signaling in inflammatory and neuropathic pain in the rat. Eur J Neurosci 19: 634-642, 2004.
79. Murray GI, Melvin WT, Greenlee WF and Burke MD: Regulation, function, and tissue-specific expression of cytochrome P450 CYP1B1. Annu Rev Pharmacol Toxicol 41: 297-316, 2001.
80. Lu Y, Nanayakkara G, Sun Y, Liu L, Xu K, Drummer CIV, Shao Y, Saaoud F, Choi ET, Jiang X, *et al*: Procaspase-1 patrolled to the nucleus of proatherogenic lipid LPC-activated human aortic endothelial cells induces ROS promoter CYP1B1 and strong inflammation. Redox Biol 47: 102142, 2021.
81. Malik KU, Jennings BL, Yaghini FA, Sahan-Firat S, Song CY, Estes AM and Fang XR: Contribution of cytochrome P450 1B1 to hypertension and associated pathophysiology: A novel target for antihypertensive agents. Prostaglandins Other Lipid Mediat 98: 69-74, 2012.
82. Singh P, Dutta SR, Song CY, Oh S, Gonzalez FJ and Malik KU: Brain Testosterone-CYP1B1 (Cytochrome P450 1B1) generated metabolite 6β-Hydroxytestosterone promotes neurogenic hypertension and inflammation. Hypertension 76: 1006-1018, 2020.
83. Yu M, Wang Z, Wang D, Aierxi M, Ma Z and Wang Y: Oxidative stress following spinal cord injury: From molecular mechanisms to therapeutic targets. J Neurosci Res 101: 1538-1554, 2023.
84. Fakhri S, Abbaszadeh F and Jorjani M: On the therapeutic targets and pharmacological treatments for pain relief following spinal cord injury: A mechanistic review. Biomed Pharmacother 139: 111563, 2021.
85. Sun L, Zhang J, Niu C, Deering-Rice CE, Hughen RW, Lamb JG, Rose K, Chase KM, Almestica-Roberts M, Walter M, *et al*: CYP1B1-derived epoxides modulate the TRPA1 channel in chronic pain. Acta Pharm Sin B 13: 68-81, 2023.
86. Falero-Perez J, Sorenson CM and Sheibani N: Cyp1b1-deficient retinal astrocytes are more proliferative and migratory and are protected from oxidative stress and inflammation. Am J Physiol Cell Physiol 316: C767-C781, 2019.
87. Lange KW and Li S: Resveratrol, pterostilbene, and dementia. Biofactors 44: 83-90, 2018.
88. Azzini E, Peña-Corona SI, Hernández-Parra H, Chandran D, Saleena LAK, Sawikr Y, Peluso I, Dhumal S, Kumar M, Leyva-Gómez G, *et al*: Neuroprotective and anti-inflammatory effects of curcumin in Alzheimer's disease: Targeting neuroinflammation strategies. Phytother Res 38: 3169-3189, 2024.
89. Ocal O, Borcek AO, Pasaoglu O, Gundogdu AC, Kaplanoglu GT and Baykaner MK: Can quercetin be an option for treatment of spinal cord injury? An experimental study. Turk Neurosurg 29: 247-253, 2019.
90. Ye G, Lin C, Zhang Y, Ma Z, Chen Y, Kong L, Yuan L and Ma T: Quercetin alleviates neuropathic pain in the rat CCI model by mediating AMPK/MAPK pathway. J Pain Res 14: 1289-1301, 2021.
91. Fakhri S, Gravandi MM, Abdian S, Moradi SZ and Echeverría J: Quercetin derivatives in combating spinal cord injury: A mechanistic and systematic review. Life (Basel) 12: 1960, 2022.
92. Hou DD, Zhang W, Gao YL, Sun YZ, Wang HX, Qi RQ, Chen HD and Gao XH: Anti-inflammatory effects of quercetin in a mouse model of MC903-induced atopic dermatitis. Int Immunopharmacol 74: 105676, 2019.
93. Gao Y, Wang Y, Wu Y and Liu S: Biomaterials targeting the microenvironment for spinal cord injury repair: Progression and perspectives. Front Cell Neurosci 18: 1362494, 2024.